Paper Title: A Comparative Study of Biomass Electrolysis and PEM Water Electrolysis for Hydrogen Production

MPhil report
Department of Chemical and Process Engineering

word count: 22653

Name: Tongao Ma

The submitted portion of this project complies with the regulations for the MPhil degree in Advanced Chemistry and Process Engineering of University of Strathclyde.

ACKNOWLEDGEMENTS

I express my sincere appreciation to all those who played a part in the successful culmination of this research paper. I am particularly grateful to my supervisor Dr. Jun Li, for offering unwavering guidance, support, and invaluable insights throughout the research process. I also appreciate the faculty members and research colleagues whose constructive feedback and encouragement greatly influenced the quality of this work. Additionally, I acknowledge the assistance from University of Strathclyde for their technical support and resources that were essential to this paper.

Last but not least, I appreciate the support, encouragement, and unwavering belief in my capabilities from my family and friends.

Each of you played a pivotal role in shaping this paper, and your contributions will forever remain a cherished part of my academic journey.

LIST OF CONTENT

Chapter 1: Introduction 1
1.1 Background 1
1.2 Aim 3
Chapter 2: Literature review 5
2.1 Hydrogen production route from fossil fuels 5
2.2 Water electrolysis 7
2.2.1 Alkaline water electrolysis 8
2.2.2 PEM water electrolysis 9
2.2.3 Solid oxide water electrolysis 11
2.3 PEM water electrolysis hydrogen production technology 13
2.4 POM-catalysed biomass electrolysis for hydrogen production 16
2.4.1 Analysis of the principle and oxidation pathway of POM-catalysed biomass electrolysis for hydrogen production 17
2.4.2 The types of biomass and molecular structures utilized for auxiliary electrolytic hydrogen generation 20
2.4.3 Homogeneous indirect oxidation of biomass 22
2.5 Research scope of this study 25
Chapter 3: Methodology 28
3.1 Reliability and basis of Aspen-Based electrolysis models 28
3.2 PEM water electrolysis - ACM model 28
3.2.1 Setup of the ACM model 33
3.2.2 Detailed explanation of parameter settings 34
3.3 POM-catalysed biomass electrolysis 38
3.3.1 Install of the Stack module 40
3.3.2 Process description 40
3.4 Model assumptions and implications 43
3.4.1 Model assumptions 43

3.4.2 Implications 46
3.4.3 Summary 47
Chapter 4: PEM water electrolysis performance analysis 48
4.1 Steady-state performance analysis 48
4.2 Dynamic response analysis 51
4.3 Chapter summary 52
Chapter 5: POM-catalysed biomass electrolysis performance analysis 54
5.1 Influence of key operating parameters 54
5.1.1 Current density (i_{cell}) 54
5.1.2 Stack temperature (T_{stack}) 56
5.1.3 Electric power input (W_{stack}) 57
5.2 Steady-state simulation results 59
5.2.1 Steady-state results 59
5.3 Performance analysis 62
5.3.1 Specific work and HTO as a function of current density 62
5.3.2 Specific work and HTO as a function of hydrogen production 64
5.3.3 Specific work and Faraday efficiency as a function of hydrogen production 65
5.3.4 Summary 66
5.4 Comparative analysis: PEM water electrolysis vs. POM-catalysed biomass electrolysis 69
Chapter 6: Comparative economic analysis 73
6.1 Simulation-based electricity cost analysis 73
6.2 Capital cost 75
6.3 Operating cost 75
6.4 Hydrogen production cost context 76
6.5 Energy efficiency 77
6.6 Technology maturity and development risk 78
6.7 Summary of economic assessment 79
Chapter 7: Outlook 81

7.1 Outlook for future research 81
7.2 Conclusion 81
Appendix 83
References 86

LIST OF TABLES

Table 3.1. Constant and cell-specific parameters in the model 32
Table 3.2. The composition of the Aspen model 33
Table 3.3. Nomenclature 37
Table 3.4. Model equipment introduction 41
Table 4.1. The steady-state simulation results 48
Table 5.1. Stream results 60
Table 5.2. Equipment sizing for major unit operations 62
Table 6.1. Capital cost component comparison. 75
Table 6.2. Qualitative operating cost comparison. 76
Table 6.3. Hydrogen production cost context and literature-based comparison 77
Table 6.4. Energy efficiency and by-product comparison. 78
Table 6.5. Technology maturity and risk comparison. 79

LIST OF FIGURES

Figure 2.1. PEM water electrolyser 14
Figure 2.2. Direct and indirect electrooxidation of lignin conversion 19
Figure 2.3. Biomass-Fe^{3+} electrolysis system 20
Figure 2.4. Molecular structure of cellulose 21
Figure 3.1. Simulation file process flow chart 33
Figure 3.2. Electric power input (W_{stack}) 35
Figure 3.3. Stack operating pressure (P_{stack}) 36
Figure 3.4. Temperature of the stack inlet stream (T_{inlet}) 37
Figure 3.5. Electrolysis diagram of common biomass 41
Figure 3.6. Process description 41
Figure 3.7. Process flow chart 43
Figure 4.1. Relation diagram of required power and hydrogen production rate 49
Figure 4.2. Voltage vs Current density 50
Figure 4.3. Partial voltage and current density relationship diagram 51
Figure 4.4. H_2 Volume flow vs. Power 52
Figure 5.1. Model-predicted effect of current density (i_{cell}) on hydrogen production and hydrogen crossover 55
Figure 5.2. Model-predicted effect of stack temperature on H_2 production and Faraday efficiency 56
Figure 5.3. Model-predicted effect of stack temperature on cell voltage and hydrogen crossover 57
Figure 5.4. Model-predicted effect of electric power input on cell voltage and current density 58
Figure 5.5. Model-predicted effect of electric power input on H_2 production and HTO58
Figure 5.6. Aspen Plus flowsheet of the H_3PO_4 -based POM-catalysed biomass electrolysis system 60
Figure 5.7. Current density vs. Specific work and HTO 63

Figure 5.8. Hydrogen production vs. Specific work and HTO 64
Figure 5.9. Hydrogen production vs. Specific work and Faraday Efficiency 65
Figure 5.10. Specific work vs. Hydrogen production 70
Figure 5.11. Cell voltage vs. Current density 71
Figure 5.12. Hydrogen production vs. Stack power input 72
Figure 6.1. Calculated electricity cost vs. H_2 production rate for PEM and POM systems 74

Abstract

This thesis presents a comparative simulation study of hydrogen production via polyoxometalate (POM)-catalysed biomass electrolysis and Proton Exchange Membrane (PEM) water electrolysis. Conventional fossil-fuel-based hydrogen production is associated with carbon dioxide emissions and environmental impacts, while water electrolysis provides a cleaner route when supplied by renewable electricity. PEM water electrolysis is commercially relevant and compatible with renewable power, but its wider application is still limited by electricity demand, noble-metal catalyst requirements, membrane cost, and stack durability.

To explore an alternative route, this study investigates POM-catalysed biomass electrolysis using cellulose as the representative biomass feedstock. In this process, POM acts as a redox mediator under acidic conditions. Biomass oxidation can replace or partially avoid the kinetically demanding oxygen evolution reaction at the anode, which may reduce cell voltage, electricity consumption, and anode catalyst requirements.

Aspen Plus and Aspen Custom Modeler were used to develop a preliminary, literature-supported process modelling framework for comparing the two routes under a consistent modelling basis. The PEM water electrolysis model was used as the reference case, while the POM-catalysed biomass electrolysis model was developed by adapting the electrolysis framework to an H_3PO_4-based acidic system containing the POM-mediated biomass oxidation pathway. The comparison focuses on key model-predicted indicators, including cell voltage, current density, hydrogen production rate, specific work, Faraday efficiency, hydrogen crossover into the oxygen stream, denoted as HTO in this study, and electricity-cost contribution. A dynamic response analysis was also carried out for the PEM system.

The simulation results indicate that, under the assumptions and representative operating conditions used in this study, POM-catalysed biomass electrolysis may reduce the electricity-related energy demand compared with PEM water electrolysis. The electricity-cost calculation also suggests a lower electricity-cost contribution for the POM-catalysed route. Overall, this thesis provides an Aspen-based comparison framework for evaluating the two electrolysis routes for hydrogen production.

Key words: POM-catalysed biomass electrolysis; PEM water electrolysis; polyoxometalate; Aspen Custom Modeler; hydrogen production.

Chapter 1: Introduction

1.1 Background

Currently, countries across the world are actively developing and implementing clean energy development strategies. In this strategic competition for energy development, in addition to energy conservation and emission reduction, the most important thing is the adjustment of the energy structure [1]. In the process of energy structure transformation, hydrogen energy is regarded as a secondary energy with great development prospects in the 21st century. This is not only because of its sustainability and regenerative capacity, but also because, compared to traditional fuels, hydrogen only produces water when burned, without generating other pollutants and greenhouse gases. Moreover, it has a higher mass energy density, allowing it to store more energy in the same volume, and it can also be combined with various green energies such as solar and wind energy, showing a high adaptability [2]. Therefore, building an energy technology system centered on hydrogen energy technology is key to accelerating global energy transformation and achieving the global "carbon neutrality" goal as soon as possible.

Hydrogen energy can be divided into three categories based on its source and the cleanliness of the hydrogen production process: "grey hydrogen," "blue hydrogen," and "green hydrogen". Grey hydrogen is obtained from traditional fossil energy sources (such as oil, natural gas, coal, etc.), and its production process emits a large amount of CO_2. Although the cost of hydrogen production is low, the carbon emission is high, making it least clean [3]. Blue hydrogen is also prepared from traditional fossil energy sources, but the production process uses CO_2 capture and storage technology to prevent CO_2 emissions into the atmosphere. Although the CO_2 emissions in this hydrogen energy technology are relatively low, the technical difficulty is high, and the cost is high, making it unsuitable for long-term development [4]. Green hydrogen is produced using electrical energy generated by renewable energy sources (such as wind energy, solar energy, hydro energy, etc.), through the electrolysis of water or biological pathways [5]. There is almost no carbon emission in this process, making it the cleanest hydrogen energy technology, but the production cost is

highest.

Electrolysis of water to produce hydrogen involves the process of decomposing water into hydrogen and oxygen under the influence of direct current electricity, which includes cathode and anode reactions. This method is highly suitable for industrial applications that require large amounts of hydrogen. The technology route does not emit CO_2 and other toxic and harmful substances, and can be driven by electrical energy generated from renewable energy sources, making it a truly "green hydrogen" production route [6]. The water electrolysis route for hydrogen production has the advantages of high efficiency and high purity, but its production cost is high, and the technical difficulty level is also high, currently only accounting for 4% of the total hydrogen production capacity globally [7]. The current technologies for water electrolysis hydrogen production mainly include alkaline water electrolysis, acidic proton exchange membrane water electrolysis, and solid oxide electrolysis water technologies [8].

Among various electrolysis technologies, PEM water electrolysis stands out due to its efficiency in splitting water molecules into hydrogen and oxygen [9]. This method involves applying an electric field to water, ionizing molecules into protons (H+) and hydroxide ions (OH-), which then migrate through the electrolyte membrane to respective electrodes, resulting in the liberation of hydrogen and oxygen gases. The electrolysis efficiency of PEM is usually about 70-80% [10], and the purity of the hydrogen produced is ideal for direct use in fuel cells [11]. These attributes position PEM water electrolysis as a leading technology for renewable energy-based hydrogen production [12].

Biomass electrolysis is an innovative approach that utilizes the conversion of biomass into hydrogen through electrolytic processes. Biomass, which includes organic materials such as plant matter and waste, serves as a renewable feedstock for this technology. Traditional PEM electrolysis, while effective, is often constrained by high operational costs and reliance on costly noble metal catalysts [13]. These catalysts are essential for facilitating the electrochemical reactions that split water into hydrogen and oxygen but can be prohibitively expensive. To mitigate these challenges, researchers have been exploring the use of POM catalysts in biomass electrolysis. POMs are a class of compounds known for their unique

catalytic properties and ability to activate and convert biomass into valuable products, including hydrogen. The application of POMs in electrolysis aims to enhance the efficiency of hydrogen production while reducing the reliance on precious metals, thus potentially lowering the overall process costs [14]. The integration of biomass catalysis with POM catalysts presents a sustainable and economically viable alternative to conventional hydrogen production methods [15]. By leveraging the abundant and renewable nature of biomass, this technology not only offers a pathway to produce hydrogen with reduced environmental impact but also promises higher yields. This makes biomass electrolysis with POM catalysts a promising avenue for advancing the field of clean energy production and contributing to a more sustainable future [16].

1.2 Aim

This research aims to provide a detailed comparison of PEM water electrolysis and POM-catalysed biomass electrolysis for hydrogen production. The main goals of this study are divided into the following three categories:

(1) **Model development and assessment**: Develop Aspen Plus and Aspen Custom Modeler models for PEM water electrolysis and POM-catalysed biomass electrolysis, and assess their reasonableness using literature-supported assumptions and material and energy balances. As shown in Chapter 3.

(2) **Efficiency and production rate comparison**: Compare the hydrogen production efficiency and rates of the two electrolysis methods. This involves analysing the steady-state responses (system performance at a stable equilibrium) of both systems and the dynamic response (transient behaviour over time) of the PEM system to compare the model-predicted performance trends of the two routes as shown in Chapters 4 and 5.

(3) **Operational parameter analysis**: Examine the impact of different operational parameters such as temperature, pressure, and reactant concentrations on the efficiency of both electrolysis methods. Identify favourable operating regions within the assumptions of the present model. As shown in Chapters 4 and 5.

Chapter 2: Literature review

2.1 Hydrogen production route from fossil fuels

As early as the early 20th century, hydrogen energy was regarded as an energy source with great development potential, and in the 21st century, hydrogen energy was more in-depth research and development as a major clean energy source. At present, the global hydrogen energy source mainly relies on traditional fossil energy (oil, natural gas and coal), and the hydrogen production from electrolytic water accounts for a relatively small proportion [17].

The principle of hydrogen production from fossil fuels is to decompose hydrocarbons in fossil fuels such as coal and natural gas into H_2 and CO_2 through high-temperature reactions. Coal gasification hydrogen production technology is one of the most economical and large-scale hydrogen production technologies. It converts coal and oxygen or steam into syngas containing H_2 and CO under high temperature conditions, and then obtains high-purity hydrogen through water-gas conversion and hydrogen purification processes [18]. The main chemical reactions that occur in the coal to hydrogen technology are as follows:

Steam mixing reaction process:

$$C + H_2O \rightarrow CO + H_2 \quad (2.1)$$

Oxygen mixing reaction process:

$$C + 1/2\ O_2 \rightarrow CO \quad (2.2)$$

Water gas conversion process:

$$CO + H_2O \rightarrow CO_2 + H_2 \quad (2.3)$$

The above water gas shift process requires catalysts. However, sulphur-containing impurities in coal-derived gas, such as H_2 S and COS, can poison conventional catalysts and reduce their activity and service life. Therefore, sulphur-resistant catalysts are commonly required for coal-based water-gas shift operation. It is reported that the Co-Mo accelerator system is widely used in the hydrogen production process of coal gasification, which has excellent sulphur poisoning resistance and wide operating temperature window [19]. However, this technology emits CO_2 and sulphur-containing gases during the production process, so its

future development is limited.

Hydrogen production from natural gas is currently the primary source of industrial hydrogen in the world. As the main component of natural gas is methane, it has the highest hydrogen-to-carbon ratio among hydrocarbons, so the hydrogen production technology using natural gas as raw material has the advantages of high hydrogen gas purity, high hydrogen production efficiency, low carbon emission, and large production scale [20]. The technology of hydrogen production from natural gas mainly includes steam reforming and catalytic cracking [21]. Natural gas steam reforming produces hydrogen by catalytically reacting methane with steam at elevated temperature and pressure. The process generally consists of three main steps: syngas generation, water gas shift conversion, and hydrogen purification. The main reactions involved are shown below.

Steam process:

$$CH_4 + H_2O \rightarrow CO + 3H_2 \quad (2.4)$$

Water gas conversion process:

$$CO + H_2O \rightarrow CO_2 + H_2 \quad (2.5)$$

The hydrogen technology of catalytic cracking of natural gas is to directly crack natural gas to obtain hydrogen under ultra-high temperature conditions and the action of catalyst, and there is no need to introduce steam and oxygen in the process [22]. The main chemical reactions in the process of catalytic cracking of natural gas for hydrogen production are as follows.

Cracking process:

$$CH_4 \rightarrow C + 2H_2 \quad (2.6)$$

Compared to steam reforming, the catalytic cracking process does not produce additional carbon emissions, but the technology is immature, and the catalyst is easily deactivated [23]. Therefore, through the development of high activity catalyst and the improvement of reactor,

the development of catalytic cracking hydrogen technology is the trend of research on natural gas hydrogen production technology. Compared with natural gas and coal hydrogen production technology, methanol hydrogen production technology has the advantages of low temperature and easy purification of hydrogen, which has been widely concerned by scholars at home and abroad [24]. Methanol hydrogen production is commonly based on steam reforming, in which methanol and steam react catalytically at elevated temperature to form syngas. The syngas is then further converted through the water-gas shift reaction to produce high-purity hydrogen. The main chemical reactions in the methanol catalytic steam reforming process are as follows.

Methanol cracking process:

$$CH_3OH \rightarrow CO + 2H_2 \quad (2.7)$$

Water gas conversion process:

$$CO + H_2O \rightarrow CO_2 + H_2 \quad (2.8)$$

There are many kinds of catalysts for hydrogen in methanol steam reforming process, including nickel, palladium and copper. Compared with natural gas and coal hydrogen production technology, methanol hydrogen production technology has the advantages of low reaction temperature, abundant raw material sources, mature technology and high hydrogen purity, but its raw material cost is high and economic advantages are not obvious [25]. Therefore, the key to the future methanol hydrogen production technology is to reduce the cost of methanol raw materials and develop efficient catalysts.

In summary, fossil energy hydrogen production technology inevitably generates and emits a large amount of carbon dioxide during the production process, so the hydrogen product obtained by this technology is also known as "grey hydrogen".

2.2 Water electrolysis

The phenomenon of electrolysis was first discovered by van Troostwijk and Diemann in 1789, experimentally using a static motor to produce electricity and discharge it on a gold

electrode in water [26]. In 1800, J. Ritter conducted a real experiment on hydroelectrolysis and collected oxygen and hydrogen [23]. At the end of the 19th century, water electrolysis entered the stage of industrial application, and electrolytic devices (using alkaline electrolysis solutions) began to be put into operation [27]. In 2022, the global water electrolyser market shipments reached 1 GW and will maintain a high growth trend [28].

Hydrogen production by electrolytic water is divided into two half-cell reactions, including oxygen evolution reaction (OER) on the anode side and hydrogen evolution reaction (HER) on the cathode side. The global reaction principle can be reduced to the equation 2.9, where E_{eq} is the equilibrium potential under standard conditions.

$$2H_2O \rightarrow 2H_2 + O_2,\ E_{eq} = 1.23\ V \quad (2.9)$$

According to the type of working electrolyte and the type of transferred ions (OH^-, H^+, and O^{2-}), the technology of electrolytic water hydrogen production is mainly divided into three categories: alkaline water hydroelectrolysis (AWE), proton exchange membrane (PEM) hydroelectrolysis and solid oxide electrolysis (SOE) [29].

2.2.1 Alkaline water electrolysis

Hydrogen production by alkaline water electrolysis is a mature technology, and the operating capacity of the electrolyser has reached the megawatt level and has been commercialized. Alkaline water electrolyser usually operates at a low temperature of 60-80 ℃, with 20-30% high concentration lye (such as KOH and NaOH aqueous solutions) as the electrolyte solution, and nickel-based non-noble metal materials are used in the anode and cathode [30]. The electrode reaction equation is shown in equations 2.10 and 2.11. The OH^- in the alkali liquor on the anode side loses electrons and oxidizes to O_2, while the H_2O molecule on the cathode side gets electrons and reduces to H_2. In addition to the anode and cathode, the key components of the alkaline electrolyser are diaphragm separators, such as asbestos, polyether sulfone (PES), microporous polymer films, glass-reinforced polyphenylene sulphide (PPS) compounds, etc., the main role is to separate the gas produced by the cathode and anode, while allowing OH^- and water molecules to penetrate [31].

Anode: $4OH^- \rightarrow O_2 + 2H_2O + 4e^-$ (2.10)

Cathode: $2H_2O + 2e^- \rightarrow H_2 + 2OH^-$ (2.11)

Although alkaline water electrolysis is one of the most commercially established electrolysis technologies and has relatively low operating costs, it still has several limitations in practical applications. First, the use of concentrated alkaline electrolytes can cause corrosion and operational degradation. During long-term operation, electrolyte leakage or loss may occur, and the stack components and diaphragm may gradually degrade, leading to reduced efficiency. In addition, the produced gas may contain alkaline mist, which requires further removal before downstream use. Second, the diaphragm cannot completely prevent gas crossover. To avoid the mixing of H_2 and O_2 and the associated safety risks, the pressure difference between the anode and cathode sides must be carefully controlled. As a result, the operating pressure of conventional alkaline electrolysers is usually limited. Furthermore, the use of liquid electrolytes and relatively thick porous diaphragms, typically around 500 μm, restricts ionic transport and limits the achievable current density and efficiency. The operating current density is generally below 600 mA cm^{-2}, and the electrolysis efficiency is typically around 60%. Another limitation is the relatively slow start-up and load response of alkaline electrolysers, together with their narrower operating range. These characteristics make them less suitable for highly fluctuating renewable power inputs, and they are therefore more commonly operated under relatively stable power conditions [32]. Based on the above shortcomings, current research in alkaline hydroelectrolysis focuses on the development of polymer films (such as anion exchange films) under alkaline conditions to replace electrolytes and membranes, and on optimizing catalyst/electrode materials to achieve higher current density, operating pressure, and a safe environment.

2.2.2 PEM water electrolysis

Proton exchange membrane water electrolysis, also known as polymer electrolyte membrane electrolysis, is also known as acid electrolysis due to the strong acidity of the

electrolyte after the anode reaction. In 1966, GE developed the first water electrolyser based on the proton conduction concept and commercialized the first water electrolyser of this type in 1978, and today commercial PEM water electrolysers operate at megawatts [33]. PEM water electrolytic cell uses a proton exchange membrane with good chemical stability, proton conductivity and gas separation to separate the anode and cathode, and the flow medium is pure water, avoiding the use of alkaline electrolyte [34]. The anode and cathode use iridium and platinum-based precious metal materials respectively. The electrode reaction is shown in equation 2.12 and 2.13. On the anode side, H_2O molecules lose electrons and undergo oxidation reaction to generate O_2 and a large amount of H+. H+ is transferred from the anode to the cathode through the proton exchange film, and electrons are obtained on the cathode side for reduction reaction to generate H_2 [35].

Anode: $4OH^- \rightarrow O_2 + 2H_2O + 4e^-$, E0 = 1.23 V vs.RHE* (2.12)

Cathode: $2H_2O + 2e^- \rightarrow H_2 + 2OH^-$, E0 = 0 V vs.RHE (2.13)

*RHE, Relative to reversible hydrogen electrode

Due to the use of precious metal catalysts, PEM electrolysis is currently more expensive than alkaline electrolysis, but exhibits some key advantages. PEM electrolytic cell system has compact design and small footprint. The polymer electrolyte membrane used allows protons as charge carriers to pass through while preventing gas transmission, and can achieve high pressure (up to 40 MPa) operation. There is no alkaline fog in the generated gas, and the purity of hydrogen can be as high as 99.999%, which is safer and more environmentally friendly. The lower film thickness (about 20-300 μm) provides good proton conductivity and low ohmic losses, allowing the electrolyser to achieve A higher current density (> 2 A/cm2) and electrolytic efficiency at 2 V, thus helping to reduce operating costs [36]. Another advantage of PEM electrolysers is their high load flexibility and ability to provide grid balancing services. Due to the low gas permeability of polymer electrolyte membranes and the rapid reaction of proton transport across the membranes to power input, rather than the inertia delay that occurs in liquid electrolytes, PEM electrolysers can operate at full range

dynamic loads (0 - 100%) [37]. In addition, the good fast start-up and response performance of PEM electrolysers also makes them ideal for direct integration with the grid and renewable solar or wind energy, and low-cost off-peak power can be used for H_2 production, which is important for reducing the disruption of existing grid operations caused by the intermittency of renewable energy generation [38]. At present, one of the main challenges of PEM electrolysis is to reduce production costs and improve energy conversion efficiency. Research on OER and HER electrocatalysts with high activity, durability and low cost, and improvement of electrolytic cell components are necessary conditions to promote the further commercial development of PEM electrolysis technology.

2.2.3 Solid oxide water electrolysis

Hydrogen production by electrolysis of water base on solid oxide has attracted much attention due to its high efficiency and environmental friendliness, which allows the storage of electrical and thermal energy from renewable sources as chemical energy (H_2) and avoids the use of precious metals as electrode catalysts [34]. In 1980, Donitz and Erdle first reported the use of supported tubular electrolytes in solid oxide electrolysers, operating at a current density of 0.3 A/cm^2, single cell voltage and energy consumption as low as 1.07 V and 2.57 kWh/m^3 for hydrogen, respectively. Additionally, faraday efficiency can reach 100% [39]. Since then, solid oxide electrolysis (SOE) has been extensively studied and is still in the laboratory development stage. The solid oxide electrolytic cell operates at a high temperature of about 500-1000 ℃, and part of the energy required for water decomposition is provided in the form of heat. The anode usually uses zirconia, and the cathode uses nickel-zirconia and strontium-doped lanthanum magnetite materials, etc. The electrode reaction is shown in equation 2.14 and 2.15. On the cathode side, H_2O molecules get electrons and undergo a reduction reaction to form H_2 and O^{2-}, and O^{2-} is transferred from the cathode to the anode through a dense solid electrolyte, where the loss of electrons occurs in an oxidation reaction to form O_2 [40]. Among them, yttria-stabilized zirconia (YSZ) is the most widely used solid electrolyte material. Due to cooling requirements, the total water consumption is approximately 83.3 times that of hydrogen production [24].

Anode: $O^{2-} - 2e^- \rightarrow 1/2\ O_2$ (2.14)

Cathode: $HO^- + 2e^- \rightarrow H_2 + O^{2-}$ (2.15)

Due to the use of solid ceramic electrolytes, solid oxide electrolytic systems can be as simple and compact as PEM electrolysers and can respond quickly. Its unique feature is that the high-temperature operating conditions require the simultaneous input of heat and power, which can be matched with external heat sources such as industrial waste heat, wind energy and solar energy, where heat replaces part of the power consumption, so the voltage and power consumption requirements of hydropower electrolysis are significantly reduced, and the electrical efficiency exceeds 80%, which can theoretically achieve 100% [41]. Solid oxide electrolysis can also operate at high pressures of up to 3 MPa and has the potential to be commercialized and used for conventional hydrogen production, as well as promising applications in the co-electrolysis of steam and CO_2 to produce syngas [42]. Long-term durability studies have reported measurable performance degradation during 1000-hour scale operation, particularly under high temperature, high steam content, and high current density. This degradation is commonly associated with microstructural changes in the electrodes, such as Ni migration, Ni agglomeration, electrode delamination, and increased ohmic resistance [43]. In addition, because O^{2-} is used as the charge carrier, the H_2 produced by the cathode will be mixed with the water vapor transported with O^{2-}, requiring additional gas separation processing to obtain high-purity hydrogen, increasing part of the capital cost [44]. Therefore, although the SOE technology has the highest electrical efficiency, it faces challenges such as safety, electrode layering, material degradation and thermal cycling, and further development is still needed. A lot of research is currently being done on reducing the operating temperature of Solid oxide electrolyte electrolytic cells and developing proton-conducting materials that exhibit high efficiency and excellent ion/proton conductivity compared to O^{2-} conductors, and electrolytic systems using proton conductors can be coupled directly to high-temperature reactor steam cycles. Pure, dry hydrogen gas is produced at the cathode [45].

2.3 PEM water electrolysis hydrogen production technology

PEM water electrolyser has the advantages of environmental friendliness, low ohmic loss, high current density and efficiency, high gas purity, compact system, fast response and large load range, and is well matched with the rapidly developing renewable power such as wind and solar power, so it is more attractive for industrial applications, and is considered to be the most promising sustainable hydrogen production technology for large-scale energy storage [46].

PEM water electrolyser is mainly composed of proton exchange membrane, anode and cathode catalyst layer (CL), anode and cathode gas diffusion layer (GDL) and flow field plate/bipolar plate (BP), etc. The working principle is as follows: Water is supplied to the electrolyser and enters the cell through the anode-side end plate. It then flows along the anode flow channels, passes through the porous anode diffusion layer, and reaches the anode catalyst layer. Under the applied DC voltage, water is oxidized at the anode to produce protons, electrons, and oxygen. The generated oxygen is removed from the cell together with unreacted water through the anode outlet, while the electrons are transferred through the external circuit. The protons migrate through the proton exchange membrane to the cathode, where they combine with electrons to form hydrogen. The produced hydrogen is then discharged through the cathode diffusion layer and flow channels. The working principle and process flow chart of PEM water electrolysis tank are shown in Figure 2.1 [44,45].

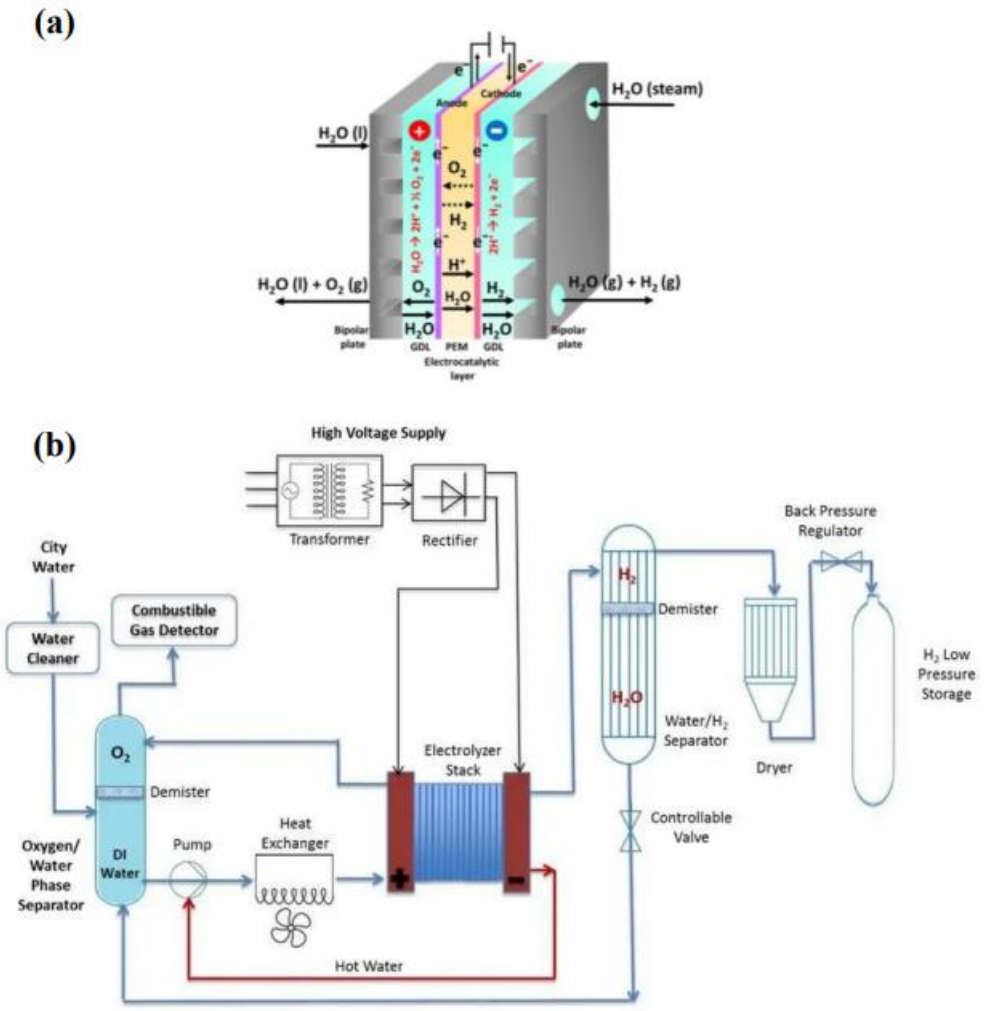

Figure 2.1. PEM water electrolyser

(a) Working principle; (b) Process flow chart. Under reversible (loss-free) conditions, the potential difference between the anode and cathode electrodes is called the reversible cell voltage (ΔErev0) and corresponds to the minimum electrical work required to decompose water in the presence of the necessary thermal energy contribution [47].

Under standard conditions (i.e., pressure P = 1 atm and temperature T = 298.15 K), the Gibbs free energy (ΔG_R^0) of the global water decomposition reaction is 236.483 kJ/mol, and the reversible battery voltage can be estimated according to equation 2.16, where n is the number of electron moles transferred by the reaction. F is the Faraday constant (96485 C/mol), and the reversible battery voltage under standard conditions is 1.229 V. When there is no external heat source, all the energy required for the reaction is transferred through electrical energy, and the reversible battery voltage at this time is called the thermo-neutral voltage

(ΔEth0), which can be estimated according to equation 2.16 and 2.17, where the enthalpy change (ΔHR0 = ΔGR0 + TΔS0) is -285.83 kJ/mol. It can be seen that the thermal-neutral voltage under standard conditions is 1.481 V.

$$E_{rev}^0 = \Delta_R^0 / nF = 1.229\ V \qquad (2.16)$$

$$E_{th}^0 = \Delta H^0 / nF = 1.481\ V \qquad (2.17)$$

However, in the actual working process of PEM electrolyser, irreversible loss of current will occur when passing through the battery, and the actual voltage of the water decomposition reaction is often higher than the reversible battery voltage. These losses can be divided into Faraday losses (activation losses) and non-Faraday losses (ohm and mass transfer losses) to model the voltage of the cell, as shown in equation 2.18, where N_c is the number of cells, E_{OCV} is the open circuit voltage, $V_{Act,a}$ and $V_{Act,c}$ are the activation over-potential of the anode and cathode, respectively. i is the current density and R_{cell} is the resistance of the electrolyser (ohmic loss). Activation loss occurs in the process of electrochemical reaction activation. At low current density, activation loss is the main reason for the decrease of battery efficiency. Ion and electron conduction resistance are the main losses of the battery during the operation of the intermediate current density. Due to the high conductivity of the plate and membrane electrode materials, only ohmic losses caused by proton transmission through PEM are generally considered. At high current density, bubbles from the reaction can block the active region, break the contact between the electrode and the electrolyte, and reduce catalyst utilization, so mass transfer loss (V_{diff}) is the main loss and current limitation is required to achieve high efficiency. In order to improve the efficiency of water decomposition, applying an over-potential to the battery is essential to overcome the electrode reaction activation energy and drive electron transfer, but high battery voltage usually means a large amount of power consumption [48].

$$V = N_c(E_{ov} + V_{Act,c} + V_{Act,a} + iR_{cell}) \qquad (2.18)$$

Some scholars have conducted economic studies on PEM electrolysis technology. The overall cost of PEM electrolyser consists of two parts: capital expenditure and operating expenditure. The capital cost is affected by H_2 production equipment (36.1%) and construction (34.3%), while the operating cost is mainly electricity consumption, accounting for about 70% of the cost of hydrogen production [49]. At present, the capital cost of PEM electrolysis system is about 4 times that of alkaline electrolyser. In order to reduce the cost of hydrogen production by PEM electrolysis, an urgent problem to be solved is to develop an efficient and economical electrode reaction catalyst, reduce the use of precious metals and improve the catalytic activity and durability of the catalyst in acidic electrolyte, so as to reduce battery overvoltage and hydrogen production energy consumption [50]. This is important to reducing both capital and operating expenses.

2.4 POM-catalysed biomass electrolysis for hydrogen production

High electricity demand is one of the key factors constraining the large-scale deployment of water electrolysis for hydrogen production, as electricity consumption directly affects operating cost and requires substantial low-carbon or renewable power supply. The theoretical voltage for water electrolysis to produce hydrogen is 1.23 V, with a theoretical electricity consumption of 2.94 kWh/m³ (under standard conditions, the same below) [51]. However, due to the presence of overpotentials and internal resistance, and to ensure a certain rate of hydrogen production in actual operation, the actual decomposition voltage reaches 2.0 to 2.2 V, resulting in an actual electricity consumption of 4.5 to 5 kWh/m³. Among these, the anodic oxygen evolution reaction (OER) is a four-electron transfer process with slow reaction kinetics and high overpotentials. Ninety percent of the electrical energy consumption in the electrolysis water system comes from the OER. By replacing the anodic oxygen evolution reaction with other reactions that can occur at lower potentials, the electricity consumption for water electrolysis to produce hydrogen can be reduced [49]. Currently, various substances are being explored to decrease the reaction potential energy required for hydrogen production through water electrolysis. Among these, biomass materials, such as cellulose and lignin, are gaining attention due to their wide availability and low cost, making them attractive for

researchers working on improving the efficiency of electrolytic processes. Taking lignin as an example, it is a natural high molecular weight aromatic polymer that accounts for about 20% to 30% of the total weight of plant bodies, with up to 150 billion tons of lignin produced annually through plant growth [52]. As a widely available and renewable carbon resource in nature that can directly provide an aromatic ring structure, the use of lignin for hydrogen production can reduce the system's hydrogen production electricity consumption while achieving the co-production of high-value chemicals. Research on biomass electrolysis for hydrogen production is of great significance for the development of low electricity consumption hydrogen production technology and the high-value utilization of biomass resources [53].

2.4.1 Analysis of the principle and oxidation pathway of POM-catalysed biomass electrolysis for hydrogen production

In general, during the water electrolysis process, oxygen evolution occurs at the anode and hydrogen evolution (HER) occurs at the cathode, as shown in reaction 2.19 ~ 2.21 [54].

Cathode reaction: $2H^+ + 2e^- \rightarrow H_2$ (2.19)

Anode reaction: $H_2O - 2e^- \rightarrow 2H^+ + 1/2O_2$ (2.20)

Overall reaction: $H_2O \rightarrow H_2 + 1/2O_2$, $\Delta G_{298K} = +237.2$ KJ/mol (2.21)

The biomass-assisted electrolytic hydrogen production system substitutes the anodic oxygen evolution reaction with a biomass oxidation reaction that can take place at a lower potential. In an ideal scenario, the biomass molecules are oxidized to CO_2, with the anodic and overall reaction equations represented as reaction 2.22 and 2.23 respectively [55]. The overall reaction equation indicates that this system fundamentally combines the chemical energy of biomass with electrical energy for hydrogen production, thus reducing the consumption of electrical energy. The theoretical voltage for water electrolysis is 1.23 V, with the energy consumption for hydrogen production being 237.2 kJ/mol. The theoretical energy consumption for hydrogen production in biomass-assisted electrolysis is merely 40.2 kJ/mol, and according to the Nernst equation, the decomposition voltage can be lowered to 0.21 V. It

is important to note that equation 2.25 is a simplified ideal reaction equation, and the oxidation of organic matter in the anodic reaction is much more complex than this equation. In the liquid phase system, the degree of biomass oxidation is low, and most organic substances are still retained in the liquid environment [56].

$$\text{Anode reaction: } 1/2C + H_2O \rightarrow 2H^+ + 1/2CO_2 + 2e^- \quad (2.22)$$

$$\text{Overall reaction: } 1/2C + H_2O \rightarrow H_2 + 1/2CO_2 \quad (2.23)$$

The oxidation of biomass at the anode is categorized into direct and indirect oxidation, with the oxidation mechanism (illustrated with lignin as an example) depicted in Figure 2.2. The direct oxidation of biomass at the anode takes place at the electrode/solution interface, which is heterogeneous. Thus, the key to enhancing this process lies in the design of efficient anode materials that facilitate effective collisions between biomass macromolecules and the electrode surface, aiming to achieve the oxidation and depolymerization of biomass macromolecules [57]. Beyond the direct oxidation route at the anode, there is also an indirect oxidation pathway mediated by hydroxyl radicals. Typical metal oxides such as PbO_2, SnO_2, and boron-doped diamond (BDD) anodes can produce hydroxyl radicals on their surfaces, which then further oxidize biomass macromolecules [58]. However, hydroxyl radicals possess an extremely potent oxidizing capacity, and upon formation, they rapidly react with organic or inorganic substances in the liquid phase, with rate constants ranging from 10^6 to 10^9 mol/(L·s), leading to a short lifespan and presence only in the vicinity of the anode surface. The indirect oxidation reactions mediated by hydroxyl radicals in the anode region are generally represented by reaction 2.24 and 2.25) where M denotes the anode [59].

$$M + H_2O \rightarrow M(HO^-) + H^+ + e^- \quad (2.24)$$

$$M(HO^-) + R \rightarrow M + mCO_2 + nH_2O + H^+ + e^- \quad (2.25)$$

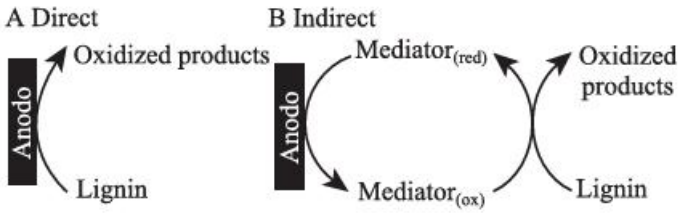

Figure 2.2. Direct and indirect electrooxidation of lignin conversion

Lignin, cellulose, and other biomass materials are high molecular weight substances with a three-dimensional, reticulated structure, which leads to slow mass transfer in liquid phase systems. Depending only on the collision of large molecules such as lignin with the anode to undergo oxidation reactions can result in slow reactions and a low current density for hydrogen production in the system [60]. To tackle this issue, researchers have suggested adding "charge transfer mediators" (i.e., redox couples) to the electrolytic system to intensify the oxidation of lignin and similar substances. The primary redox couples used in current research include Fe^{3+}/Fe^{2+} and polyoxometalates (POMs). As depicted in Figure 2.3, after the addition of Fe^{2+} to the anode, the main reaction that occurs is the oxidation of Fe^{2+} (reaction 2.26), and the Fe^{3+} generated subsequently oxidizes the biomass in the anode region's solution and is reduced back to Fe^{2+}, as shown in reaction 2.27. By incorporating the Fe cycle, the oxidation reaction of biomass macromolecules is shifted from the anode interface to the anode region's solution [61].

Anode reation: $Fe^{2+} - e^- \rightarrow Fe^{3+}$ (2.26)

Anode liqid phase: $Fe^{3+} + \text{biomass} \rightarrow Fe^{2+} + \text{oxidized biomass}$ (2.27)

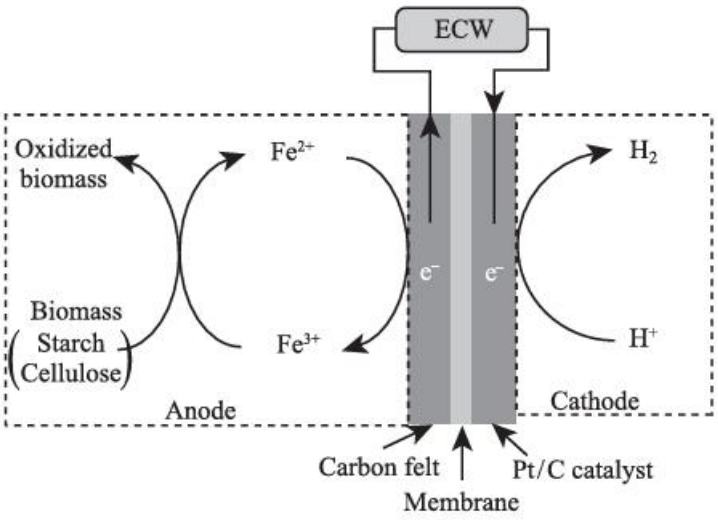

Figure 2.3. Biomass-Fe^{3+} electrolysis system

In summary, the oxidation paths of biomass in biomass water electrolysis hydrogen production technology mainly include: (1) the direct oxidation pathway at the anode, (2) the indirect oxidation pathway facilitated by hydroxyl radicals generated at the anode, and (3) the indirect oxidation pathway through "charge transfer carriers" such as Fe^{3+} or POMs. In the case of the direct oxidation pathway of biomass, it depends on the physical impact between the biomass and the anode, and it is usually necessary for the electrolyte temperature to reach between 80 – 180 °C to achieve a more desirable current density, hydrogen production rate, and biomass oxidation depolymerization rate at a low cell voltage [62].

2.4.2 The types of biomass and molecular structures utilized for auxiliary electrolytic hydrogen generation

In the current research on biomass-assisted electrolytic water splitting, the primary biomass feedstocks include carbohydrate substances such as cellulose, which is composed of glucose units, and lignin, which is rich in aromatic ring structures [63]. Hemicellulose is seldomly used in research for assisting electrolytic water splitting because it has a lower yield than cellulose and lignin, and it holds greater value for alternative applications. The use of biomass in electrolytic water splitting can substitute the anodic oxygen evolution reaction with the oxidation reaction of biomass in the anode region. This approach can, on one hand, reduce the cell voltage and achieve hydrogen production with lower energy consumption [64].

On the other hand, it can leverage the oxidation of biomass to produce high-value organic compounds, such as alcohols and small molecule organic acids.

Cellulose is a high molecular weight polysaccharide made up of D-glucose units, with a simplified molecular equation of $(C_6H_{10}O_5)_n$, and it is the most abundant natural polymer in the world. Its production materials can come from a variety of sources such as wood, cotton, reeds, and mulberry bark, which are widely available and inexpensive, making it a precious natural renewable resource [65]. The structure of cellulose is depicted in the following Figure 2.4. However, in comparison to other water-soluble substances, cellulose has a hard crystalline structure and poor water solubility, which cannot be directly and effectively oxidized by the anode. Thus, the introduction of "charge transfer carriers" is necessary [66]. The cellulose molecule is abundant in functional groups such as alcohol hydroxyl and ether bonds, which can be oxidatively depolymerized by Fe^{3+} or POM in the solution, resulting in the formation of small molecule substances such as carboxylic acids [67].

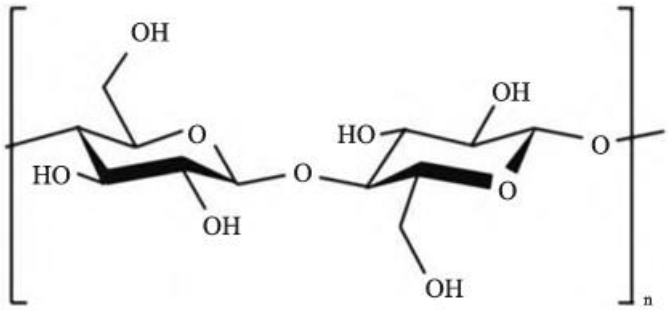

Figure 2.4. Molecular structure of cellulose

Lignin is found in all plants except for mosses and fungi, and it is the second most abundant natural organic polymer after cellulose. It is widely available, inexpensive, and is anticipated to become one of the primary sources of aromatic compounds in the future [68]. The structural unit of lignin is the phenylpropane molecule, which is linked by carbon-carbon bonds (C-C) and ether bonds (C-O-C) to form a high molecular weight polymer. The main structural units include guaiacyl (G), syringyl (S), and p-hydroxyphenyl (H) propane units. The C-C linkages primarily consist of four types: β-5, α-O-4, β-β, and β-1, while the C-O-C linkages mainly include four types: β-O-4, α-O-4, α-O-γ, and 4-O-5 [69].

Besides the high molecular weight biomass discussed above, some researchers also categorize small molecule alcohols like methanol and ethanol, as well as glucose, as biomass and incorporate them into the anode to aid in electrolytic hydrogen production. These small molecule substances are soluble in water and easily diffusible, leading to a more desirable enhancement in hydrogen production compared to high molecular weight biomass [70].

2.4.3 Homogeneous indirect oxidation of biomass

The homogeneous indirect oxidation of biomass necessitates the introduction of "charge transfer carriers" in the anode area, which serve as redox mediators within the solution. In the electrochemical system for the indirect oxidation of biomass, the "charge transfer carrier" is initially oxidized at the anode and subsequently oxidizes the biomass in the liquid phase in an irreversible manner. Consequently, the selection of "charge transfer carrier" directly impacts the cell voltage needed for the electrochemical system and the efficacy of biomass oxidation. The "charge transfer carriers" frequently utilized at present are POMs, Fe^{2+}/Fe^{3+}, and the $[Fe(CN)_6]^{4-}$/ $[Fe(CN)_6]^{3-}$ redox pair, among others [71].

POMs can activate hydrogen peroxide or oxygen molecules to facilitate the oxidation and depolymerization of lignin. Acting as a catalyst, under aerobic conditions, POMs oxidize lignin and subsequently produce a reduced form (POM_{Red}), which can be regenerated to the oxidized state POMs (POM_{Ox}) in the presence of oxygen. Deng and colleagues integrated POMs into a fuel cell system, utilizing POMs as a catalyst to develop low-temperature biomass fuel cells, converting low-temperature biomass energy into electrical energy [72]. Furthermore, Deng and colleagues introduced POMs into a biomass electrolysis system, employing graphite felt as the anode and Pt/C as the cathode in a proton exchange membrane electrolyser (PEMEC). The biomass-POMs solution, after being subjected to a heat pretreatment, is introduced into the anode region for electrolysis. Utilizing glucose as the biomass feedstock, a current density of 200 mA/cm² can be achieved at a cell voltage of only 0.28 V, which is an 83.3% energy saving compared to water electrolysis, and its hydrogen production energy consumption index is superior to that of heterogeneous oxidation of biomass on the electrode surface [73]. The anode reaction involves the oxidation where POM_{Red} loses electrons, eliminating the need for a metal catalyst. The relevant reaction

equations are as follows:

$$\text{Anode reation: H-POM}_{Red} \rightarrow \text{POM}_{ox} + H^+ + e^- \quad (2.28)$$

$$\text{Cathode raction: } H^+ + e^- \rightarrow 1/2H_2 \quad (2.29)$$

$$\text{Anode liquid phase: } xH_2O+\text{biomass}+y\text{POM}_{ox} \rightarrow y\text{H-POM}_{Red}+\text{oxidized products}+CO_2 \quad (2.30)$$

Phosphomolybdic acid ($H_3PMo_{12}O_{40}$, a member of POMs) was employed as a catalyst for the oxidation and depolymerization of biomass, and conducted electrolytic hydrogen production following a pre-heating treatment with phosphomolybdic acid and lignin [74]. At a cell voltage of 0.95 V, they achieved a current density of 10 mA/cm². The primary oxidation product in the liquid phase of the anode region was vanillin, and a certain amount of CO was released during the pre-heating process. The product in the cathode region was hydrogen gas. In summary, the use of POMs as "charge transfer carriers" for the electrocatalytic oxidation and depolymerization of biomass offers several advantages: (1) Compared to conventional electrolytic water systems, the electrolytic voltage is lowered, leading to reduced energy consumption; (2) POMs serve as electron-proton shuttles, capturing electrons from biomass and protons from water or biomass, which allows the oxidation of biomass to take place in the liquid phase instead of on the electrode surface, thus eliminating the need for noble metal electrodes and substantially reducing system costs; (3) Solar energy and the chemical energy from biomass are converted and stored in H-POM complexes within the electrolyte; (4) POMs are cost-effective and exhibit tolerance to most organic and inorganic pollutants, enabling stable electrocatalytic oxidation [75].

Apart from POMs, Fe^{3+}/Fe^{2+} is another frequently utilized "charge transfer carrier." Dong Lichun and colleagues employed a proton exchange membrane electrolyser, incorporating the Fe^{3+}/Fe^{2+} ion pair into the biomass electrolysis system, with graphite felt serving as the anode [73]. Hydrogen could be generated at a temperature of 90°C and a cell voltage of 0.7 V, which is lower than the cell voltage of any electrolytic water system that uses precious metals. In the glucose-Fe^{3+} system, at a current density of 0.1 A/cm², the cell voltage was merely 0.72 V, and the energy consumption for hydrogen production was 1.845

kWh/Nm³, which is a 60.7% energy saving compared to the electrolytic water system at the same current density. Additionally, the anode did not require the use of precious metals, as the anode reaction involved the oxidation of Fe^{2+} [76].

Deng and colleagues utilized a Proton Exchange Membrane Electrolyser (PEMEC) for the electrolytic production of hydrogen from lignin, incorporating the Fe^{3+}/Fe^{2+} redox pair and employing pure graphite felt as the anode. The researchers accomplished hydrogen production from lignin-assisted electrolyzed water through a two-step approach: initially, Fe^{3+} was blended and heated with lignin, followed by the introduction of the heated mixture into the anode region for electrolysis. At a current density of 0.1 A/cm², the anode potential was approximately 0.8 V (relative to the reversible hydrogen electrode), with the energy consumption for hydrogen production being 2.30 kWh/Nm³. Lignin underwent depolymerization via electrochemical oxidation, resulting in the formation of gaseous CO_2 and CH_4 (in relatively small quantities). A significant portion of the lignin did not react, and the primary products from the lignin that did participate in the reaction through oxidation and depolymerization included vanillin, 4-methylbenzaldehyde, and benzoic acid [67].

The incorporation of Fe^{3+}/Fe^{2+} imposes certain requirements on the anode region's electrolyte, requiring that the anode solution be kept under acidic conditions. However, natural lignin is only soluble in strong alkaline solutions and sulfite solutions. Thus, in the electrolytic system that employs Fe^{3+}/Fe^{2+}, lignin must undergo pretreatment, or alternative industrial by-products of lignin should be considered [47]. The precise mechanism behind the oxidation of lignin remains unknown, but the shearing mechanism of its oxidative depolymerization can be explored by examining the reductive functional groups of lignin and the products that result from its depolymerization [24].

In conclusion, the incorporation of "charge transfer carriers" such as POMs or Fe^{3+}/Fe^{2+} relocates the oxidation reaction of biomass from the electrode surface to a homogeneous liquid phase system. This method increases the efficiency and degree of biomass oxidation compared to heterogeneous oxidation systems, thus supplying a greater number of electrons. Additionally, the introduction of "charge transfer carriers" changes the anode reaction from the oxidation of biomass to that of Fe^{2+}, which does not necessitate the use of noble metal

catalysts. This enables the employment of cost-effective electrode materials such as graphite felt, further reducing the system's costs.

Although biomass-assisted electrolysis shows considerable potential for reducing the electrical energy demand of hydrogen production, existing research still has several limitations. Most studies remain at the laboratory scale and mainly focus on reaction mechanisms, catalyst activity, or single-cell electrochemical performance, while process-level modelling and system-level evaluation are still limited. In addition, the complex and variable composition of biomass feedstocks makes it difficult to establish a universal kinetic model, especially when different biomass types, intermediates, and oxidation pathways are involved. Practical issues such as POM catalyst stability, catalyst recycling, biomass pretreatment, product separation, and long-term operation also require further investigation. Therefore, current studies provide valuable mechanistic and experimental evidence, but they are not yet sufficient to evaluate the overall process performance, energy demand, and economic potential of biomass electrolysis under a consistent comparison framework. This limitation justifies the need for a process-level modelling study. Accordingly, this thesis uses Aspen Plus and Aspen Custom Modeler to develop a preliminary, literature-supported simulation framework for comparing POM-catalysed biomass electrolysis with PEM water electrolysis in terms of hydrogen production, specific work, operating parameters, and preliminary economic implications.

2.5 Research scope of this study

This report focuses on the comparison of two hydrogen production technologies: Proton Exchange Membrane (PEM) water electrolysis and polyoxometalate (POM) catalysed biomass electrolysis. Traditional fossil-fuel-based hydrogen production routes are associated with carbon emissions and environmental impacts, while conventional water electrolysis still faces challenges such as high electricity consumption, high material cost, membrane durability issues, and dependence on precious metal catalysts. Therefore, it is necessary to investigate alternative electrolysis routes that may reduce energy demand and improve the

economic potential of hydrogen production.

PEM water electrolysis is selected as the reference system in this study because it is a representative low-temperature water electrolysis technology with high hydrogen purity, high current density, compact system design, and good compatibility with renewable electricity. However, its large-scale application is still constrained by electricity demand and the use of expensive catalyst and membrane materials. In comparison, POM-catalysed biomass electrolysis provides a biomass-assisted route for hydrogen production. In this system, cellulose is used as the biomass feedstock, while POM acts as a redox catalyst under acidic conditions. Biomass oxidation can replace or partially avoid the kinetically demanding oxygen evolution reaction at the anode, thereby providing a potential route for reducing cell voltage, electricity consumption, and anode catalyst requirements.

Previous experimental research has shown that POM-catalysed systems can significantly reduce the required cell potential for electrolysis under acidic conditions. For example, Liu Wei reported that the use of a POM catalyst could decrease the required cell potential from approximately 1.8 V to 0.67 V [69]. This finding provides an experimental basis for considering POM-catalysed biomass electrolysis as a promising alternative route. However, most existing studies remain focused on reaction mechanisms, catalyst behaviour, or laboratory-scale electrochemical performance, while process-level modelling and systematic comparison with established PEM water electrolysis are still limited.

To address this gap, Chapter 3 develops an Aspen Plus and Aspen Custom Modeler based simulation framework for comparing PEM water electrolysis and POM-catalysed biomass electrolysis. The PEM model is used as the reference case, while the biomass electrolysis model is developed by adapting the electrolysis framework to an H_3PO_4-based acidic system containing the POM-mediated biomass oxidation pathway. The analysis focuses on key indicators such as cell voltage, current density, hydrogen production rate, water consumption, specific work, Faraday efficiency, and preliminary electricity-cost implications. For the PEM water electrolysis system, dynamic response behaviour is also examined to evaluate changes in voltage, current, and hydrogen production under changing operating conditions. Sensitivity analysis is carried out to examine how key operating parameters affect

system performance. The purpose of this study is therefore to provide a preliminary, literature-supported, system-level comparison of the two routes.

Chapter 3: Methodology

3.1 Reliability and basis of Aspen-Based electrolysis models

Following the research scope defined in Section 2.5, Aspen Plus and Aspen Custom Modeler were selected as the main simulation tools for developing the comparative process model in this study. These tools allow electrochemical equations, thermodynamic calculations, stream connections, and process-level performance indicators to be integrated within a consistent simulation environment. This is important for comparing PEM water electrolysis and POM-catalysed biomass electrolysis under a common modelling framework.

Previous Aspen-based electrolysis modelling studies have reported reasonable agreement between simulation results and experimental or literature data for key performance indicators, including hydrogen production rate, oxygen production rate, cell voltage, stack power, and specific energy consumption [77-78]. These studies suggest that Aspen Plus and Aspen Custom Modeler can provide a useful modelling basis for electrolysis systems when appropriate governing equations, operating assumptions, and thermodynamic parameters are applied. Therefore, these references are used in this thesis to support the selection of Aspen-based modelling tools rather than to provide a separate literature review.

In this study, the PEM water electrolysis model is first constructed as the reference case. The modelling framework is then adapted to describe the H_3PO_4-based, POM-catalysed biomass electrolysis system, in which POM functions as a redox mediator for biomass oxidation under acidic conditions. The model is used to compare the two hydrogen production routes in terms of cell voltage, current density, hydrogen production rate, specific work, Faraday efficiency, and preliminary electricity-cost implications. For the PEM water electrolysis system, dynamic response behaviour is also examined to evaluate changes in voltage, current, and hydrogen production under changing operating conditions.

3.2 PEM water electrolysis - ACM model

$$V_{cell} = V_{id} + V_{act} + \Delta V_{ohm} + \Delta V_{diff} \quad (3.1)$$

In which, V_{id} refers as the ideal voltage (V);

The ideal voltage V_{id} relates to the alteration in Gibbs free energy of the reaction $2H_2O \rightarrow 2H_2 + O_2$, plus a pressure correction. Here, F refers as Faraday's constant and γ_{H_2O} is the activity of water.

V_{cell} refers as cell membrane potential, which represents the difference between the potential inside and outside the cell.

V_{act} refers as activation potential, usually refers to the potential change of a cell under certain stimulation (such as action potential).

Δ_{ohm} refers as Ohmic voltage loss, usually related to the resistance of an electric current through a cell membrane or tissue.

Δ_{diff} refers as Nutrient distribution voltage or diffusion voltage, which represents the potential difference caused by the difference in the limit concentration of ions or molecules in the cell membrane.

$$V_{id} = \frac{\Delta G^{\circ}(T_{stack,}, P_{stack})}{nF} + \frac{RT_{stack}}{nF} \ln\left(\frac{\rho_{H_2}\rho_{O_2}^{0.5}}{\gamma_{H_2O}}\right) \tag{3.2}$$

The activation overpotential is computed for both cathode and anode. In equation 3.3, α_X isthe charge coefficients and $i_{0,X}$ is the exchange current densities.

$$\Delta V_{act,} = \frac{RT}{\alpha_X nF} \ln\left(\frac{i_X}{i_{0,X}}\right) \tag{3.3}$$

The ohmic overpotential is a result of both the resistance presented by the electrodes and the PEM itself. In equation 3.4, A is the cell area.

$$\Delta V_{ohm} = (R_{electrodes} + R_{mem}) i_{useful} A \tag{3.4}$$

The electrode resistance is computed from resistivity and thickness.

$$R_{electrodes} = R_{anode} + R_{cathode} = \frac{t_{an}\rho_{an}}{A} + \frac{t_{cat}\rho_{cat}}{A} \tag{3.5}$$

The membrane resistance is significantly larger than electrode resistance and is computed from a conductivity σ_{mem} (S/cm) which is estimated with the Springer model:

$$R_{mem} = \frac{t_{men}}{\sigma_{mem} A} \tag{3.6}$$

$$\sigma_{mem} = (0.005139\lambda - 0.00326)\exp\left(1268\left(\frac{1}{303} - \frac{1}{T_{stack}}\right)\right) \tag{3.7}$$

Note the influence of the Faraday efficiency, which defines a "useful" current density. The efficiency is taken to be constant at $\eta F = 0.99$.

$$i_{useful} A = I_{stack}\eta_F \tag{3.8}$$

Finally, diffusion losses are computed for the anode side only, using a limiting current term. Diffusion losses are orders of magnitude smaller than the other losses computed above and could also be ignored.

$$\Delta V_{diff} = \frac{RT}{\alpha_{an} nF} \ln\left(\frac{i_L}{i_L - i_{an}}\right) \tag{3.9}$$

The above equations are implicit in i_{cell} and are solved simultaneously with ACM.

The stack input power W_{stack} is fixed in the simulation.

$$W_{stack} = V_{cell} i_{cell} A_{cell} N_{cells} \tag{3.10}$$

The extent of reaction follows from the current density as mentioned above.

$$nF\dot{N}_{H_2} = i_{useful} A N_{cells} \tag{3.11}$$

Three mechanisms facilitate the movement of water across the membrane. Water may be dragged from anode to cathode by electro-osmotic forces ($F\dot{N}^{eo}_{H2O}$) (This flow is positive from anode to cathode.).

$$F\dot{N}^{eo}_{H2O} = n_d i_{useful} A N_{cells} \tag{3.12}$$

where the coefficient n_d is a function of the membrane hydration λ (see Table 3.1).

$$n_d = 0.0029\lambda^2 + 0.005\lambda - 3.4x10^{-19} \tag{3.13}$$

Diffusion losses are again very small because the difference in water concentration across the membrane is practically negligible. In ACM, the water concentrations are computed with a flash on the anode and cathode sides. (This flow is positive from anode to cathode.)

$$\dot{N}^{diff}_{H2O} = \frac{D^{eff}_{H2O} \ (C_{H2O,an} - C_{H2O,cat}) A N_{cells}}{t_{mem}} \tag{3.14}$$

The effective diffusivity is a function of the membrane porosity (see Table 3.1). Note that the corrected native diffusivity function given in Botsis has been used, but the porosity dependence from Colbertaldo has been:

$$D^{eff}_{H2O} = D_{H2O}\varepsilon^{1.5} = 1.25x10^{-15} \exp\left[2416\left(\frac{1}{T_{amb}} - \frac{1}{T_{op}}\right)\right] \varepsilon^{1.5} \tag{3.15}$$

The cathode side generally operates at a higher pressure than the anode. The counterflow, driven by pressure, across the membrane counteracts the electro-osmotic losses. In the model sign convention, this flow is defined as positive from the cathode to the anode. The

cathode-side density and viscosity on the cathode side are computed with Aspen Properties. The Darcy permeability of the membrane, K_{Darcy}, is 1.58×10^{-18} m^2.

$$\dot{N}_{H2O}^{hydr} K_{Darcy} A_{cell} = \frac{\rho_{H2O,\ cat}(P_{cat} - P_{an})}{\mu_{H2O} t_{mem}} \tag{3.16}$$

The mass balance is resolved by considering the quantities of H_2 and O_2 produced at the cathode and anode respectively, the water loss due to electrolysis, and the movement of water across the membrane.

The energy balance assumes that all material leaving from both the cathode and anode are at a common operating temperature T_{op}. The stack is assumed to operate adiabatically apart from a minor loss of heat due to free convection of ambient air.

The heat transfer calculation is not described very well in the references. For the present model, the heat transfer coefficient is estimated with the following rule of thumb.

$$h = 1.37\left(\frac{T_{op} - 10 - T_{amb}}{L}\right)^{1.4} \tag{3.17}$$

The exterior surface temp is assumed to be 10°C below the operating temperature of the stack. The characteristic length L in equation 17 is taken as the square root of A_{cell}. The exterior area available for heat transfer is specific to the configuration and physical dimensions of the stack. To generalize the exterior area, it has been scaled to the cell area (the factor of 0.22 follows from Botsis's geometry.)

$$A_{ext} = 0.22 A_{cell} N_{cells} \tag{3.18}$$

The heat loss from the PEM stack is thus:

$$Q_{loss} = h A_{ext}(T_{op} - 10 - T_{amb}) \tag{3.19}$$

Table 3.1. Constant and cell-specific parameters in the model

Parameter description	Value

Exchange current density (anode)	$i_{o,an}=1\times10^{-10}$ A/cm^2
Exchange current density (cathode)	$i_{o,cat}=1\times10^{-3}$ A/cm^2
Charge transfer coefficient (anode)	$\alpha_{an}=0.5$
Charge transfer coefficient (cathode)	$\alpha_{cat}=0.5$
Faraday efficiency	$\eta_F=0.99$
Active cell area	$A_{cell}=160$cm^2
Number of cells	$N_{cells}=12$
Electrode resistivity	$\rho_{el}=7.5$mΩ-cm
Electrode thickness	$t_{el}=1.3$mm
Membrane thickness	$t_{mem}=127$μm
Membrane hydration	$\lambda=22$
Membrane porosity	$\varepsilon=0.3$
Membrane permeability	$K_{Darcy}=1.58\times10^{-18}$m^2

3.2.1 Setup of the ACM model

The PEM stack V12 model was installed into the Aspen plus model library. The process flow chart is displayed as follow.

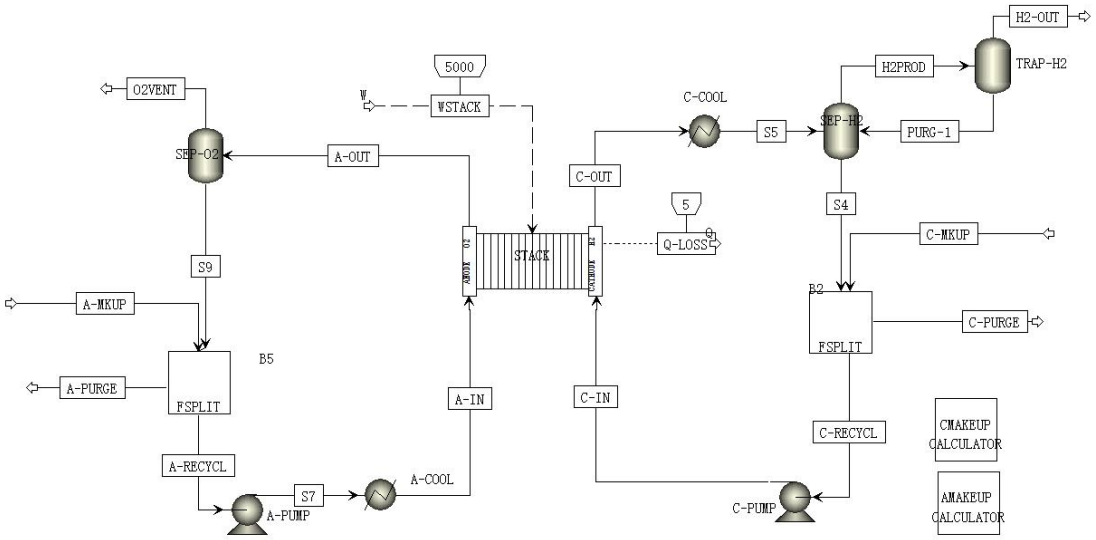

Figure 3.1. Simulation file process flow chart

Table 3.2. The composition of the Aspen model

Tag / Name	Type	Function
A-MKUP	Feed stream	Anode-side makeup gas input (typically air or O_2)
FSPLIT (left)	Flow splitter	Controls anode off-gas recycle/purge ratio
A-PURGE	Vent stream	Anode-side gas purge outlet
A-RECYCL	Recycle stream	Recycles anode off-gas
A-PUMP	Pump	Pressurizes recycled anode gas
A-COOL	Heat exchanger	Cools recycled anode gas before stack entry
A-IN	Inlet stream	Anode inlet to electrolyser stack
STACK	Electrolyser stack	Core PEM stack where water is split into H_2 and O_2
A-OUT	Outlet stream	Anode outlet containing O_2 and unused gases
SEP-O2	Separator	Separates oxygen from anode gas stream
O2VENT	Vent	O_2 vent to atmosphere
WSTACK	Power input	Electrical power input to the stack (e.g., 5000 W)
C-MKUP	Feed stream	Cathode-side water makeup stream
FSPLIT (right)	Flow splitter	Controls cathode off-gas recycle/purge ratio
C-PURGE	Vent stream	Cathode-side purge outlet
C-RECYCL	Recycle stream	Recycles cathode off-gas
C-PUMP	Pump	Pressurizes recycled cathode stream
C-IN	Inlet stream	Cathode inlet to electrolyser stack
C-OUT	Outlet stream	Hydrogen-rich cathode outlet from stack
C-COOL	Heat exchanger	Cools hydrogen-containing stream before separation
S5	Intermediate stream	Intermediary between cooler and separator
SEP-H2	Gas-liquid separator	Separates hydrogen gas from water/impurities
H2PROD	Hydrogen product	Hydrogen gas outlet from separator
TRAP-H2	Hydrogen trap	Collects dry, purified hydrogen
H2-OUT	Product stream	Final hydrogen product outlet
PURG-1	Waste stream	Wastewater or purge from hydrogen separator
Qloss	Energy loss unit	Represents heat loss from the stack (e.g., 5 units)
CMAKEUP CALCULATOR	Calculator block	Calculates required cathode water makeup
AMAKEUP CALCULATOR	Calculator block	Calculates required anode gas makeup

3.2.2 Detailed explanation of parameter settings

In the present study, three key parameters were systematically varied to investigate their influence on the electrochemical and thermal performance of H_3PO_4 electrolysis system.

These parameters include: Electric power input (W_{stack}), stack operating pressure (P_{stack}) and temperature of the stack inlet stream (T_{inlet}).

3.2.2.1 Electric power input (W_{stack})

Electric power input (W_{stack}) represents the total electrical energy supplied to the phosphoric acid electrolyser stack. It directly governs the electrochemical reaction rate and, consequently, hydrogen generation. In practical electrolysis systems, the operating variable that is actively controlled is typically the current density (i_{cell}), while the cell voltage and stack power are measured outputs determined by the electrochemical kinetics and ohmic behavior of the system.

However, in the present Aspen Plus simulation framework, W_{stack} is adopted as the independent variable. This approach enables consistent evaluation of the electrolyser's performance under varying electrochemical loads, as the model internally computes the resulting i_{cell} and V_{cell} based on the specified power input. Varying W_{stack} thus effectively emulates changes in current density while maintaining numerical stability in the steady-state calculation

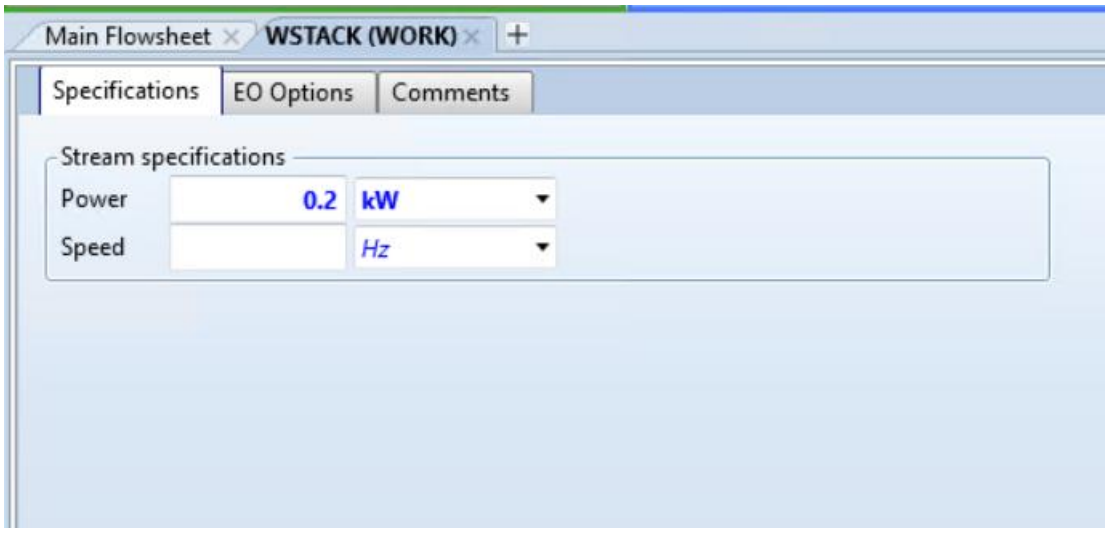

Figure 3.2. Electric power input (W_{stack})

3.2.2.2 Stack operating pressure (P_{stack})

The stack pressure (P_{stack}) defines the total operating pressure within the electrolysis system. Pressure influences both the thermodynamics and transport phenomena of the process.

An increase in pressure enhances gas solubility and improves phase separation efficiency, thereby supporting higher hydrogen partial pressures at the cathode. However, elevated pressure can also increase overpotential and compression work, potentially reducing the system's overall energy efficiency.

In this study, P_{stack} was varied from 3 to 11 bar. This range reflects practical conditions reported for medium-temperature electrolysers and allows assessment of trade-offs between hydrogen purity and energy consumption.

```
INLET as input molefractionport;
OUTcathode as output molefractionport;
OUTanode as output molefractionport;
WSTACK as input Workport;
QLOSS as output heatport;

Pstack as Pparam (value:7, description:"Stack Pressure", units:"bar");
```

Figure 3.3. Stack operating pressure (P_{stack})

3.2.2.3 Temperature of the stack inlet stream (T_{inlet})

The stack inlet temperature (T_{inlet}) represents the temperature of the process stream entering the electrolyser. It determines the initial thermal boundary condition of the stack and directly affects electrolyte conductivity, activation kinetics, and cell voltage.

In real operation, the *stack temperature* (T_{stack}) evolves dynamically due to heat generation and dissipation within the system. Therefore, in the simulation, T_{inlet} is specified as the controlled variable, while T_{stack} is an internal response that varies with operating conditions. Adjusting T_{inlet} enables investigation of thermal effects on electrochemical performance and system efficiency without imposing artificial constraints on heat transfer behavior.

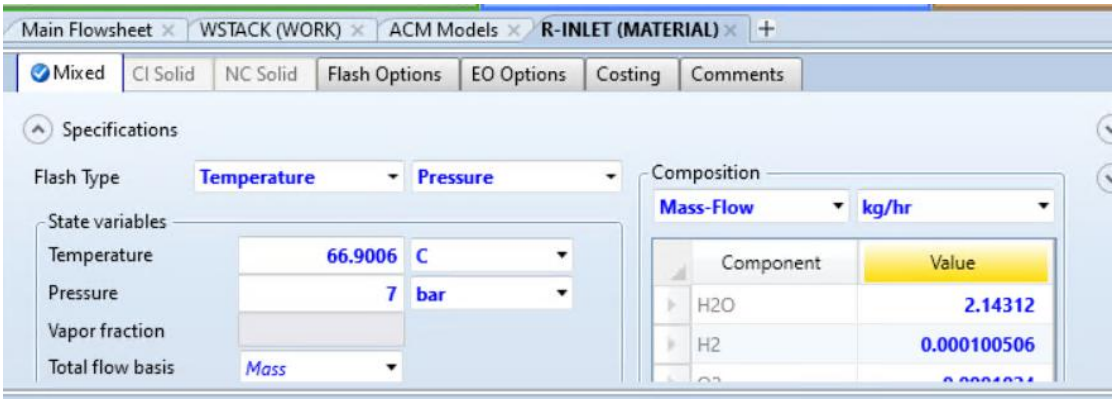

Figure 3.4. Temperature of the stack inlet stream (T_{inlet})

Table 3.3. Nomenclature

Symbol	Description	Unit
Primary Variables		
V_{cell}	Cell voltage	V
i_{cell}	Current density of electrolyser cell	$A \cdot cm^{-2}$
W_{stack}	Electric power input to electrolyser stack	W
P_{stack}	Operating pressure of electrolyser stack	bar
T_{stack}	Stack operating temperature	°C or K
T_{inlet}	Temperature of inlet stream to stack	°C or K
T_{amb}	Ambient temperature	°C or K
nH_2	Molar flow rate of H_2 produced	$mol \cdot s^{-1}$
HTO	Hydrogen crossover (mole fraction of H_2 in O_2 stream)	—
ηF	Faradaic efficiency	—
ζ	Extent of electrolysis reaction	$mol \cdot s^{-1}$
Constants		
F	Faraday constant	96,485 $C \cdot mol^{-1}$
R	Universal gas constant	8.314 $J \cdot mol^{-1} \cdot K^{-1}$
n	Number of electrons transferred per reaction (2 for H_2)	—
Voltage Components (Overpotentials)		
Vid / Vrev	Ideal (reversible) cell voltage	V
Vact	Activation overpotential	V
ΔVohm	Ohmic overpotential (voltage loss)	V
ΔVdiff	Diffusion (concentration) overpotential	V
Thermodynamic & Kinetic Terms		
ΔG / ΔG∘	Gibbs free energy change	$kJ \cdot mol^{-1}$
ΔH / ΔHr	Enthalpy change of reaction	$kJ \cdot mol^{-1}$
αan ,αcat	Charge transfer coefficient (anode, cathode)	—
i0,an ,i0,cat	Exchange current density (anode, cathode)	$A \cdot cm^{-2}$
iL	Limiting current density	$A \cdot cm^{-2}$

γH_2O	Activity of water	—
Resistance & Transport Terms		
Relectrodes	Electrical resistance of the electrodes	Ω
Rmem	Ohmic resistance of the membrane	Ω
σmem	Membrane ionic conductivity	$S \cdot cm^{-1}$
ρel	Electrode resistivity	mΩ·cm
DH_2Oeff	Effective diffusivity of water in membrane	$m^2 \cdot s^{-1}$
KDarcy	Membrane permeability	m^2
λ	Membrane hydration (water content)	—
ϵ	Membrane porosity	—
μH_2O	Viscosity of water	Pa·s
Geometric & Stack Terms		
A_{cell}	Active area of a single cell	cm^2
N_{cell}	Number of cells in stack	—
tel	Electrode thickness	mm
tmem	Membrane thickness	μm or cm
L	Characteristic length for heat transfer	m
Aext	Exterior surface area of stack for heat loss	m^2
Heat Transfer Terms		
Qloss	Heat loss from the stack to surroundings	W
Qf / QlossF	Fraction of reaction heat lost to surroundings	—
h	Heat transfer coefficient	$W \cdot m^{-2} \cdot K^{-1}$
Semi-Empirical Model Parameters		
r,d,s,t	Empirical parameters for V_{cell} correlation	various
f	Empirical parameters for ηF correlation	various
C,E	Empirical parameters for HTO correlation	various

3.3 POM-catalysed biomass electrolysis

While the PEM water electrolysis model described in Section 3.2 provides a literature-supported reference framework for standard electrolysis, it is not directly suitable for simulating the POM-catalysed biomass electrolysis process. This is because the two systems differ in electrolyte composition, anodic reaction pathway, and feedstock characteristics. Therefore, a modified model was developed in this study to represent the POM-catalysed biomass electrolysis system under the defined modelling assumptions.

This modified model uses the core framework of the PEM model as a foundation but incorporates targeted changes to reasonably represent the main electrochemical and process characteristics of the biomass-assisted system. The justifications for this approach and the specific modifications are as follows:

Core framework reusability: The biomass electrolysis process shares a fundamental architecture with PEM water electrolysis, including the electrolytic cell configuration, the core electrochemical framework, and the logic of proton transport. Both systems revolve around proton migration and H2 generation. This similarity makes the PEM modelling framework a useful starting point and avoids the need to reconstruct the basic model architecture from the beginning.

Addressing key differences: The core differences between the two systems are concentrated in the electrolyte, the catalytic mechanism, and the raw material (feed) network.

Specific modifications: To account for these differences, the standard PEM model was modified along three key dimensions to create the new biomass electrolysis model:

Feed and Component Library: The feed system was reconfigured. Components required for biomass and the H_3PO_4 electrolyte itself were added to the component library. This includes supplementing the standard H_2O, H+, and O_2 components with the new H_3PO_4 and biomass-related compounds.

Reaction Kinetics: The reaction kinetics equations were revised to reflect the POM-catalysed reaction pathway instead of the standard water-splitting reaction. This involves embedding catalyst activity factors specific to the POM system.

Thermodynamics and Transport: The thermodynamic and proton transfer parameters were adapted. This included adjusting the proton transfer coefficient within the electrolytic cell to match the proton migration efficiency of the H3PO4 system, ensuring the model is consistent with the actual characteristics of the POM/H3PO4 catalytic electrolyte.

In summary, by retaining the core electrochemical logic of the PEM model and implementing targeted modifications to the components, reaction description, and physical property parameters, this study developed a reasonable and internally consistent simulation framework for POM-catalysed biomass electrolysis. The model is used to support

process-level comparison with PEM water electrolysis and to identify performance trends under the same modelling basis. All subsequent simulations for biomass electrolysis were conducted using this modified Aspen Plus and Aspen Custom Modeler framework.

3.3.1 Install of the Stack module

The customized electrolysis stack model (Stack1.atmlz) developed in Aspen Custom Modeler (ACM) forms the core of this simulation. Detailed instructions for its installation and verification are provided in **Appendix A.**

3.3.2 Process description

The concept of biomass electrolysis is shown in Figure 3.5. The proton exchange membrane is sandwiched between a simple graphite felt anode, not coated with any catalyst and carbon. The cathode was coated with Pt black catalyst (4 mg/cm^2) for hydrogen evolution.

The biomass is mixed with an acid solution and electrolysis is performed by applying electricity to the anode and cathode potentials (as shown in the Figure 3.6). The description of main blocks and streams is shown in Table 3.3.

At the same time, the resulting biomass-POM solution was pumped into the anode and the acidic aqueous solution (1 mol/L) was pumped into the cathode side electrolytic cell. During the electrolysis process, the reduced POM is gradually electrically oxidized and turns back to yellow. Hydrogen is released from the cathode outlet and collected. Experimentally, the biomass-POM solution can be irradiated in situ or heated in an electrolytic cell to produce hydrogen during circulation.

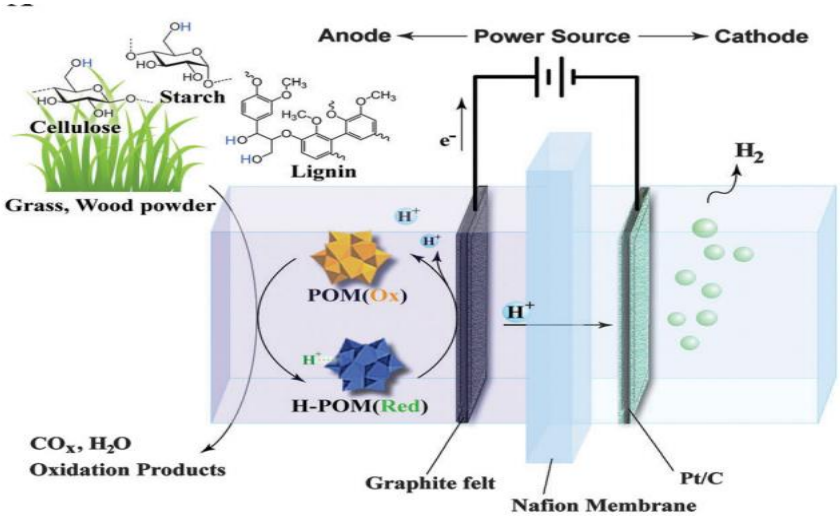

Figure 3.5. Electrolysis diagram of common biomass

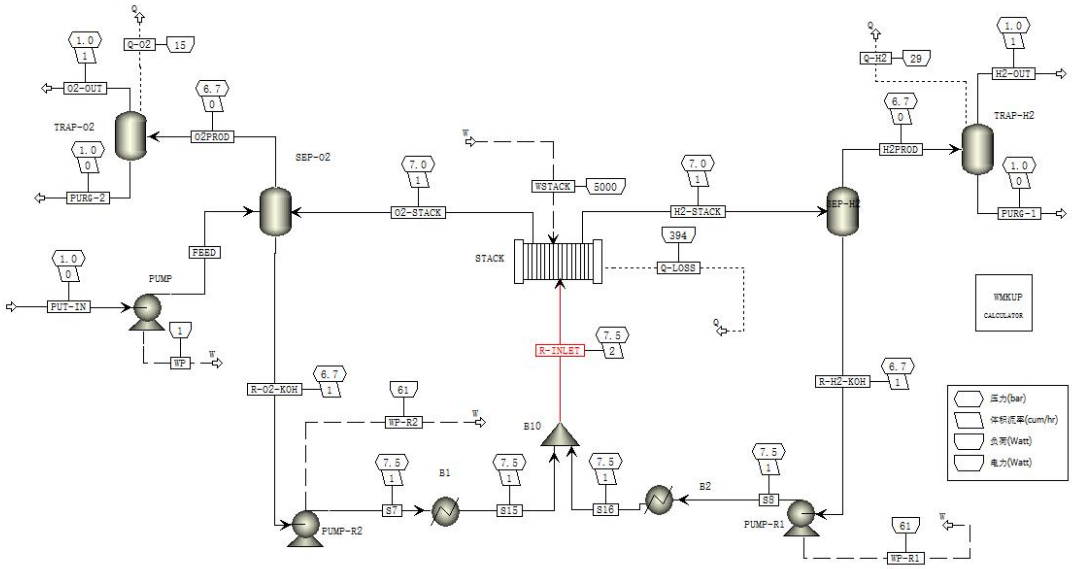

Figure 3.6. Process description

To clarify the structure of the Aspen Plus flowsheet shown in Figure 3.6, the main model blocks and stream labels are summarised in Table 3.4. The table links each Aspen component label to its corresponding process function, including feed delivery, electrolyte circulation, electrolysis reaction, gas–liquid separation, product collection, and purge control. This information is provided to help identify how the process units are connected in the simulation and how the electrolysis stack is integrated with the surrounding auxiliary units.

Table 3.4. Model equipment introduction

Component Name	Label	Function Description

Feed Pump	PUMP	Delivers feed water into the system under pressure
Raw Water Inlet	PUT-IN	Entry point of raw water
Water Pre-treatment Outlet	WP	Supplies treated water for separation or reaction
Phosphoric Acid Circulation Pump	PUMP-R2	Circulates phosphoric acid solution
Heat Exchangers	S7, S8, S15, S16	Regulate temperature of electrolytes
Mixers	B1, B2, B10	Combine electrolyte streams before entering the stack
Electrolyser Stack	STACK	Core electrochemical unit representing hydrogen evolution and the anodic oxidation process
Stack Inlet	R-INLET	Electrolyte feed point to the stack
Hydrogen Separator	SEP-H2	Separates hydrogen gas from electrolyte
Oxygen Separator	SEP-O2	Separates oxygen gas from electrolyte
Hydrogen Trap Tank	TRAP-H2	Temporarily stores hydrogen, removes impurities
Oxygen Trap Tank	TRAP-O2	Temporarily stores oxygen, removes impurities
Hydrogen Product Outlet	H2PROD	Output of purified hydrogen gas
Oxygen Product Outlet	O2PROD	Output of purified oxygen gas
Hydrogen Outlet	Q-H2	Final H_2 flow/pressure measurement point
Oxygen Outlet	Q-O2	Final O_2 flow/pressure measurement point
Hydrogen Purge Valve	PURG-1	Releases excess or impure hydrogen
Oxygen Purge Valve	PURG-2	Releases excess or impure oxygen
Stack Power Loss Monitor	Q_{loss}	Measures internal energy losses in the stack
Water Flow Meters	WP-R1, WP-R2, WSTACK	Monitor water flow into and within the system
Stack Water Feed	FEED	Feeds water to the anode side of the stack
Stack Hydrogen Outlet	H2-STACK	Hydrogen gas output from cathode side
Stack Oxygen Outlet	O2-STACK	Oxygen gas output from anode side
Electrolyte Monitoring Points	R-H2, R-O2	Monitor phosphoric acid parameters
Power Supply to Stack	5000W	Electrical input to drive electrolysis

Fresh supplementary water is added from the in stream on the left. R-INLET is used to set the mass fraction of H_2O, H_3PO_4in the circulating liquid. Since H3PO4 do not participate

in the electrolysis reaction, the two components do not need to add. Only within the internal loop, the concentration of H_3PO_4can be adjusted on the input stage.

The simulation was developed by implementing the 19 governing equations from the literature in Aspen Custom Modeler (ACM). The model equations were then solved using the numerical solver available in the software. A simplified process flow chart of the simulation procedure is shown below:

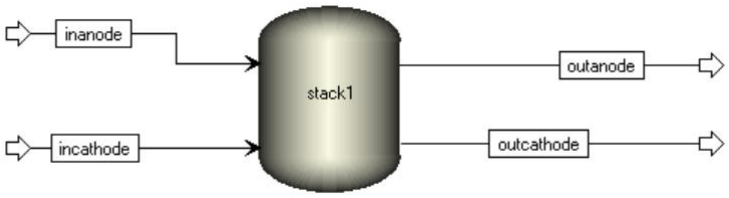

Figure 3.7. Process flow chart

At the anode, oxygen gas is generated, while at the cathode, hydrogen gas is produced. After the simulation is completed in ACM, and the results can be calculated and the module can be exported to Aspen Plus for use. In Aspen Plus, there are two main parameters to be changed, one is the current density, and the other is the input power W_{stack}.

Four main graphs are introduced in the literature: (a). current density vs. total cell voltage (V_{cell}); (b). current density vs. individual partial voltages; (c). T input power vs. hydrogen production rate; and (d). hydrogen production rate vs. specific work.

3.4 Model assumptions and implications

3.4.1 Model assumptions

a. **Core Modelling Framework**

The present work adopts the steady-state system-level modelling approach established by Sánchez [77], where the alkaline electrolysis process is represented in Aspen Plus by integrating an ACM electrochemical model.

In this study, the original KOH electrolyte model was modified to represent an H_3PO_4 based system, introducing adjustments to electrolyte-related parameters such as Electrical parameters and Faradaic-efficiency coefficients.

b. **Major Assumptions**

To enable the implementation of an electrolysis model within Aspen Plus, several simplifying assumptions were required.

These assumptions are consistent with previous alkaline electrolysis (AEL) modelling studies, Sánchez [77], Sánchez [78] and Abdin [79], and have been adapted to the phosphoric acid (H_3PO_4) electrolyte system.

(1). Steady-state

Only steady-state conditions are simulated. Transient effects, such as startup or dynamic power fluctuations, are excluded.

This allows focusing on the equilibrium performance and avoids uncertainties in time-dependent parameters, which will be addressed in future dynamic studies.

(2). Mass balance

The Faraday efficiency, η_F, is used to calculate the extent of the electrolysis reaction, $H2O -> H2 + \frac{1}{2}O2$:

$$\zeta = \frac{\eta_F \cdot i_{\text{cell}} \cdot A_{\text{cell}} \cdot N_{\text{cell}}}{2F} \tag{3.20}$$

where F is the Faraday constant (96,485 C/mol), and the factor of 2 reflects the two electrons required to produce one molecule of hydrogen.

The H3PO4 and unreacted water are equally divided between the cathode and anode outlets. Oxygen generated during electrolysis is fully assigned to the anode outlet, along with a minor portion of hydrogen as determined by the HTO crossover. The remaining hydrogen exits through the cathode outlet. Any hydrogen or oxygen initially dissolved in the inlet stream is conserved and incorporated into the respective anode or cathode flows.

(3). Enthalpy Balance

The cell stack is assumed to operate adiabatically, except for a small fraction of heat lost to the surroundings. This ambient loss is proportional to the reaction heat generated, taken as 0.288 GJ/kmol (corresponding to the enthalpy of formation of liquid water). In the ACM model, the loss fraction, Q_f, is a user-defined parameter and is set to 10% in the present study:

$$Q_{loss} = Q_f \zeta \Delta H_r \quad (3.21)$$

The remaining reaction heat, together with the electrical power input, is incorporated into the total enthalpy of the product streams.

(4). Cell Voltage

The cell voltage is calculated using a semi-empirical relation combining reversible voltage (V_{rev}), ohmic overpotentials, and activation terms as functions of current density, temperature, and pressure.

$$V_{cell} = V_{rev} + (r1 + d1 + r2T_{stack} + d2P_{stack})i_{cell} + s\log_{10}[(t1 + \frac{t_2}{T_{stack}} + \frac{t_3}{T_{stack}^2})i_{cell} + 1] \quad (3.22)$$

(5). Faraday Efficiency (η_F)

Faraday efficiency is derived from experimental AEL data [78]. These correlations implicitly account for electrolyte concentration, temperature, and pressure effects, but assume that other secondary electrochemical phenomena are negligible

$$\eta_F = (\frac{i_{cell}^2}{f_{11} + f_{12}T_{stack} + i_{cell}^2}) \cdot (f_{21} + f_{22}T_{stack}) \quad (3.23)$$

(6). HTO

Hydrogen crossover into the oxygen stream, denoted as HTO in this study, is expressed as the mole fraction of H_2 in the anode-side oxygen stream. HTO is estimated using a semi-empirical correlation based on stack temperature, pressure, and current density, following the approaches reported by Sánchez [77] and Abdin [79]. This correlation treats hydrogen crossover as a function of macroscopic operating conditions and does not explicitly resolve spatial variations, local concentration gradients, or transient diffusion effects within the electrolyte.

$$HTO = (C_1 + C_2T_{stack} + C_3T_{stack}^2 + (C_4 + C_5T_{stack} + C_6T_{stack}^2)\exp((C_7 + C_8T_{stack} + C_9T_{stack}^2)/i_{cell})) + (E_1 + E_2P_{stack} + E_3P_{stack}^2 + (E_4 + E_5P_{stack} + E_6P_{stack}^2)\exp((E_7 + E_8P_{stack} + E_9P_{stack}^2)/i_{cell}) \quad (3.24)$$

3.4.2 Implications

The assumptions outlined above have several important consequences for the interpretation and limitations of the simulation results.

The steady-state assumption simplifies the system by neglecting transient phenomena such as startup, shutdown, or fluctuating power input. Consequently, the results reflect equilibrium performance only, and any dynamic effects on voltage, temperature, or mass transport are not captured. This ensures computational efficiency and clarity in understanding the system under constant operating conditions, but dynamic behavior will need to be addressed in subsequent studies when implementing Aspen Dynamics.

The treatment of mass balance using Faraday efficiency and HTO crossover provides a semi-empirical but practical estimate of the distribution of hydrogen and oxygen between the cathode and anode streams. By assuming uniform division of H3PO4 and water between the two electrodes and incorporating a simplified model for HTO, the simulation can predict overall gas production and purity. However, localized variations, minor side reactions, or transient diffusion effects are not captured, potentially underestimating small-scale deviations in outlet compositions.

The adiabatic assumption with a fixed ambient heat loss fraction simplifies the energy balance by combining reaction heat and electrical input into the product enthalpy. While this allows for straightforward calculation of stack temperature and energy requirements, it assumes perfect thermal homogeneity and neglects any spatial temperature gradients, which could influence reaction kinetics or local cell performance in real systems.

Finally, the semi-empirical correlations for cell voltage, Faraday efficiency, and HTO enable robust predictions of electrochemical performance across a range of operating temperatures, pressures, and current densities. These correlations, derived from experimental AEL data, implicitly account for electrolyte concentration effects but assume that secondary electrochemical phenomena are negligible. Therefore, while the model is suitable for system-level optimization and comparative studies, caution should be taken when extrapolating results to extreme operating conditions or scaling up to industrial applications.

3.4.3 Summary

In summary, the electrolysis model employs several well-defined assumptions to balance realism with computational tractability. Steady-state operation, semi-empirical correlations for voltage, Faraday efficiency, and HTO, along with simplified mass and energy balances, enable consistent estimation of hydrogen and oxygen production under controlled operating conditions. The adiabatic assumption with a small ambient heat loss fraction and uniform distribution of H_3PO_4 and water between electrodes further simplifies the system while preserving key thermodynamic and electrochemical behaviors.

These assumptions collectively allow the model to serve as a reasonable process-level tool for system-level performance analysis, parametric studies, and optimization of the H_3PO_4 electrolysis process. At the same time, they highlight the limitations of the current approach, particularly the exclusion of dynamic effects, spatial heterogeneities, and minor secondary electrochemical phenomena, which will need to be addressed in future dynamic or scale-up studies.

Chapter 4: PEM water electrolysis performance analysis

This chapter analyses the performance of the PEM water electrolysis model developed in Chapter 3. The simulation was used to obtain both steady-state and dynamic response results for the model. The analysis is divided into the system's steady-state performance characteristics and its transient behaviour in response to a power change.

4.1 Steady-state performance analysis

The model was first run to a steady state to establish a baseline and confirm its stability. When the difference between the two iterations of the circulating stream is less than the set value, the model is considered to have reached a steady state. The steady-state simulation outcomes align with anticipated results, which proves the feasibility of the established PEM water electrolysis model. The primary steady-state results are shown in Table 4.1.

Table 4.1. The steady-state simulation results

Input variables	**Output variables**
pressure：2.5 atm	Current density：7.1 A/cm^2
temperature：55 °C	Hydrogen production rate：0.015 mol/s
Inlet water flow：0.1 mol/s	pressure drop：0.1 atm

With the steady-state model established, the relationship between key operating parameters was analysed.

Figure 4.1 shows the relationship between the hydrogen production rate and the specific work (energy consumption) required.

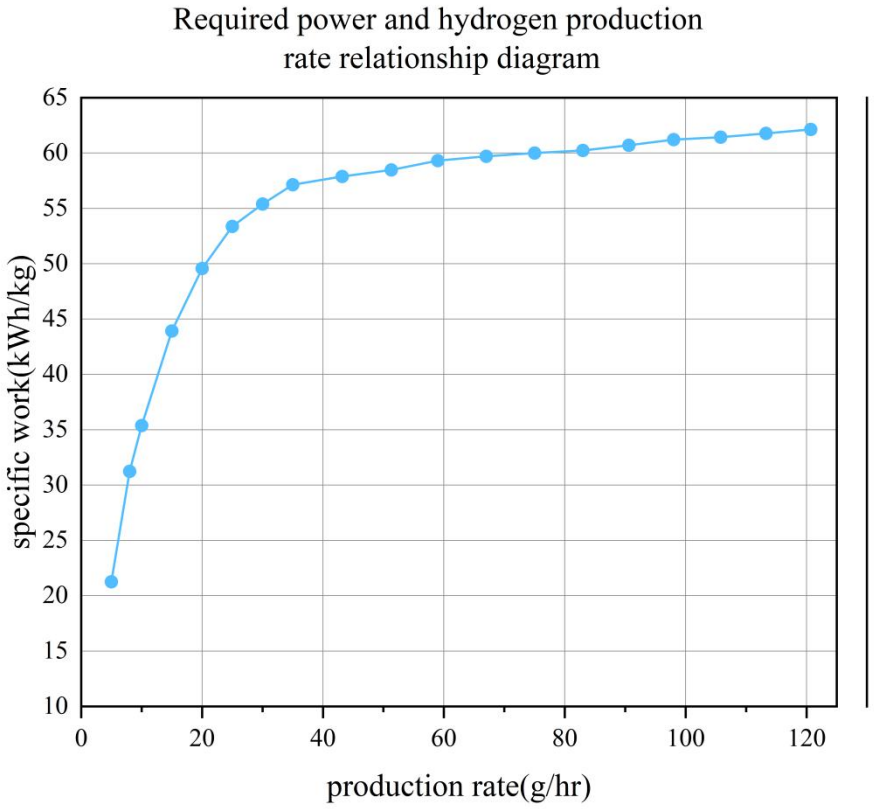

Figure 4.1. Relation diagram of required power and hydrogen production rate

As shown in the plot, when the production rate is low, the specific work required is high, indicating lower efficiency. As the production rate increases, the specific work curve flattens, stabilizing around 60-62 kWh/kg. This trend highlights the importance of operating the electrolyser at an optimal production scale to achieve higher energy efficiency and reduce production costs.

Figure 4.2 presents the model's simulated polarization curve, a key indicator of electrochemical performance.

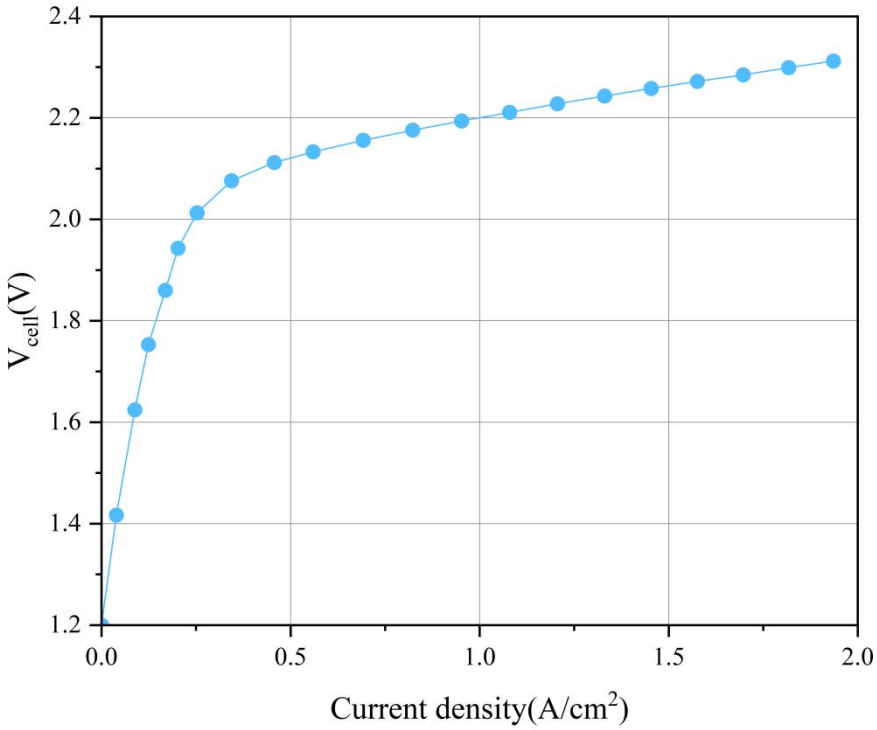

Figure 4.2. Voltage vs Current density

The polarization curve reveals the relationship between cell voltage and current density. As shown in the figure, the cell voltage increases with rising current density. The curve exhibits three distinct regions as expected:

Activation Polarization: At low current densities (<0.25 A/cm²), the rapid voltage rise reflects activation losses.

Ohmic Polarization: In the intermediate range (0.25–1.5 A/cm²), the linear increase indicates resistive losses.

Concentration Polarization: At higher current densities (>1.5 A/cm²), the curve steepens again due to mass transport constraints.

This behavior underscores the trade-off between hydrogen production rate and energy efficiency in water electrolysis systems.

Figure 4.3 shows the relationship between the individual voltage components and the current density.

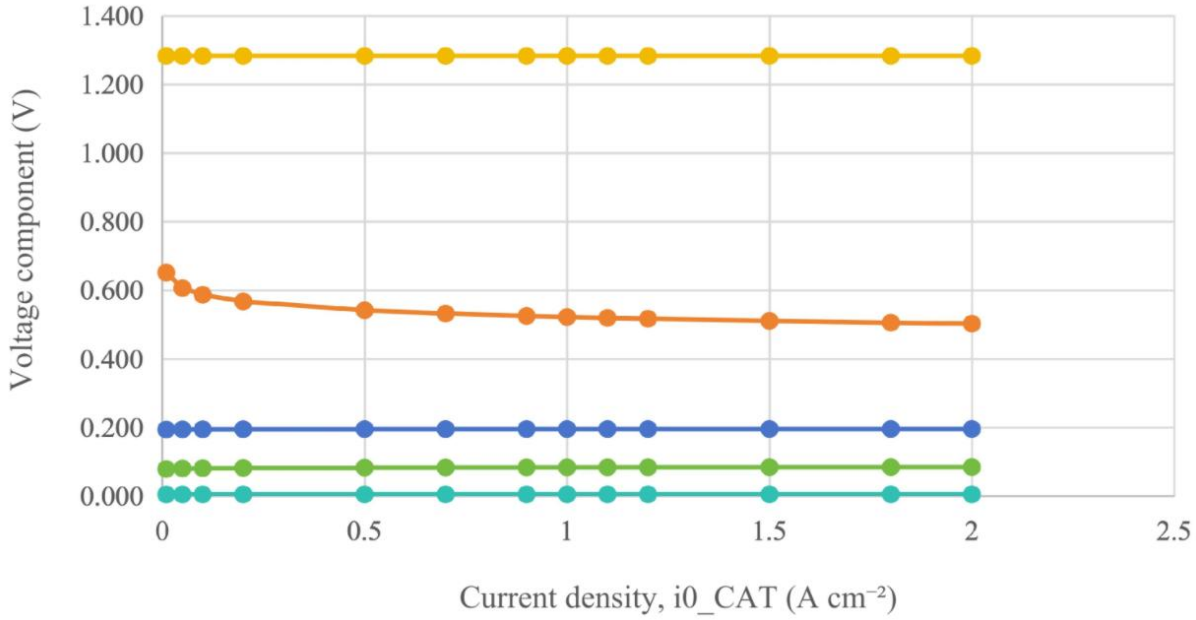

Figure 4.3. Partial voltage and current density relationship diagram

This graph analyses the different components of the total cell voltage. The curves show that as current density increases, the partial voltages remain relatively constant after an initial change. The stability of these curves at higher current densities indicates that the electrochemical reaction has stabilized, which is crucial for evaluating the performance and efficiency of different electrode materials or electrolyte systems.

4.2 Dynamic response analysis

Figure 4.4 shows the resulting hydrogen volume flow over time.

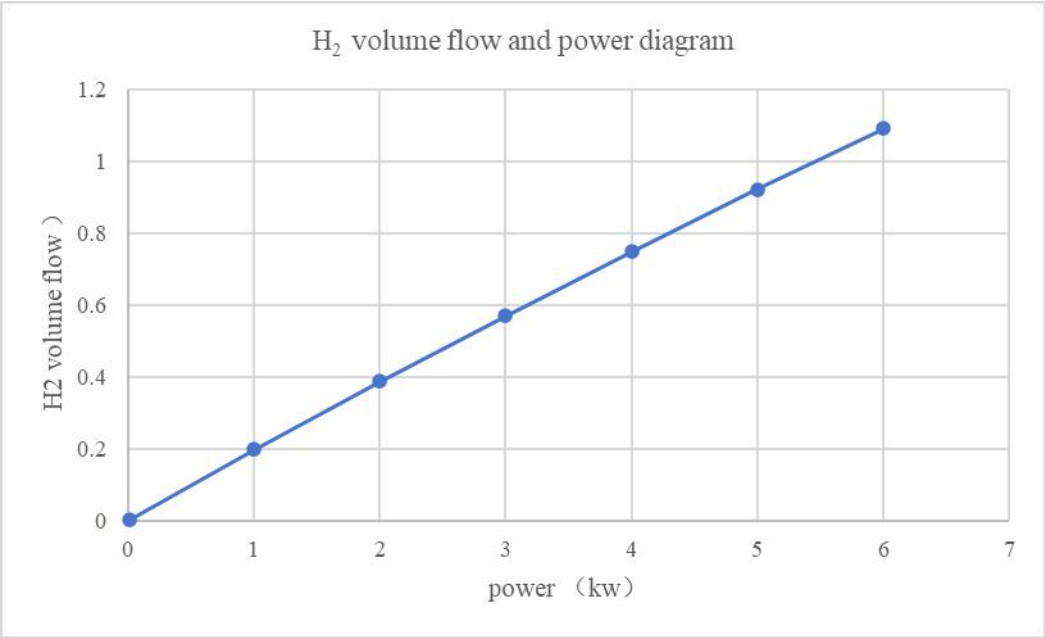

Figure 4.4. H_2 Volume flow vs. Power

This plot demonstrates a near-perfect linear relationship between the electrical energy input and the resulting hydrogen production. This behaviour is expected and aligns with Faraday's Law, where the amount of hydrogen produced is directly proportional to the total electrical charge (current*time) supplied to the system, assuming a stable voltage. This confirms the model's internal consistency and its adherence to fundamental electrochemical laws.

4.3 Chapter summary

The analyses in this chapter provide valuable insights into the performance of the PEM water electrolysis system.

Efficiency Optimization: Fine-tuning the electrolyser's design and operational parameters is necessary to sustain a stable voltage across fluctuating current densities, thereby boosting the overall system efficiency.

Production Rate Enhancement: The system is capable of scaling up its output without a proportional increase in power usage, making the most of the electrolyser's capabilities and minimizing the energy expended per unit of hydrogen generated.

Power Management: There is a crucial need for power management to align power

inputs with production goals, ensuring a balance between cost-effectiveness and sustainability in hydrogen production.

These evaluations are instrumental in formulating a comprehensive approach to refine PEM water electrolysis systems, propelling the progression of hydrogen as a clean energy carrier.

Chapter 5: POM-catalysed biomass electrolysis performance analysis

5.1 Influence of key operating parameters

The sensitivity analysis aims to evaluate the influence of key operating parameters on the performance of the H_3PO_4 based electrolysis system. This assessment is crucial for understanding the robustness of the model, identifying critical factors affecting hydrogen production, and guiding future optimization or scale-up studies.

In this study, three key operating parameters were selected for sensitivity analysis based on their physical significance and their use in previous modelling studies by Sánchez [77] and Abdin [79]. These parameters are stack temperature (T_{stack}), b. current density (i_{cell}) and c. electric power input (W_{stack}).

5.1.1 Current density (i_{cell})

The effect of current density (i_{cell}) on hydrogen production and hydrogen crossover (HTO) was analysed using the semi-empirical ACM model for the H_3PO_4 -based electrolysis stack. Current density is a key operational parameter in electrochemical systems, directly influencing reaction rates, electrode overpotentials, and mass transport phenomena.

The simulation results in Figure 5.1 show a nonlinear relationship between current density, H_2 production rate, and hydrogen crossover into the oxygen stream (HTO). No directly comparable experimental dataset was found for the same H_3PO_4 -based POM-catalysed biomass electrolysis system under the operating range considered here. Therefore, the results in Figure 5.1 are interpreted as model-predicted sensitivity trends.

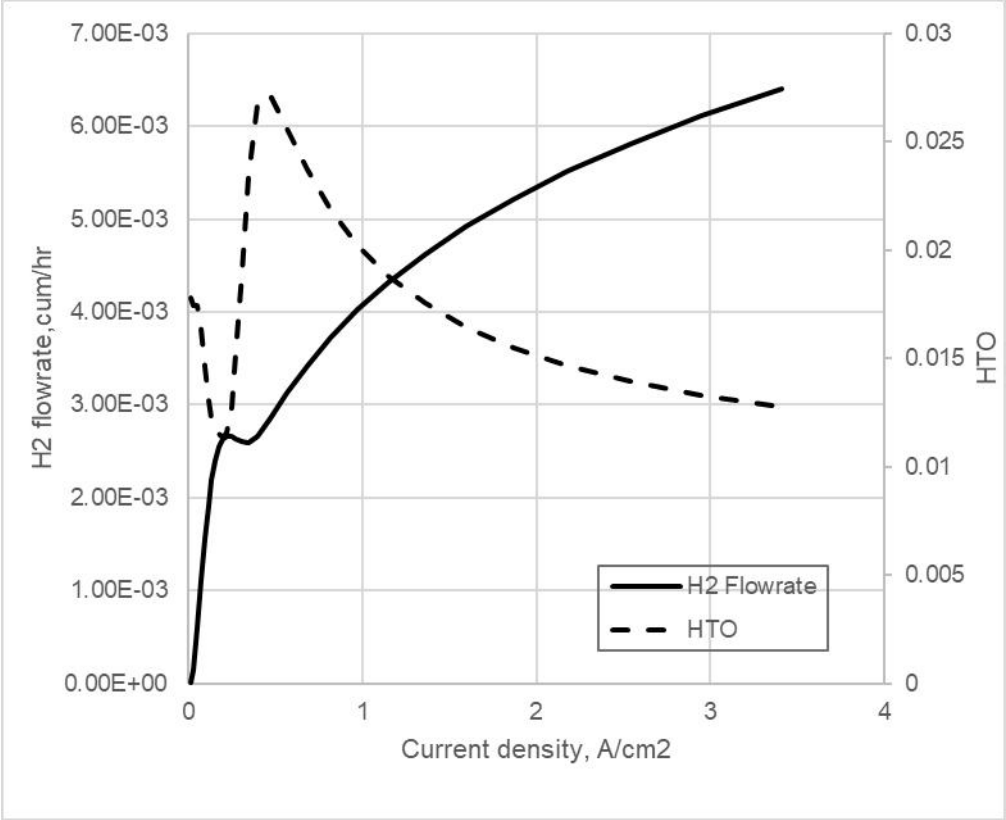

Figure 5.1. Model-predicted effect of current density (i_{cell}) on hydrogen production and hydrogen crossover

Hydrogen production

The model predicts that H_2 production generally increases with increasing current density, which is consistent with the expected electrochemical relationship between current and hydrogen generation. A slight local decrease is observed at intermediate current density values before the production rate increases again at higher current density. This non-monotonic behaviour may result from the combined influence of the semi-empirical voltage, transport, and crossover correlations used in the model. In particular, increased current density can enhance hydrogen generation, but it can also intensify ohmic and mass-transfer limitations in the H_3PO_4-based electrolyte system. The local decrease should therefore be treated as a model-predicted sensitivity feature rather than a confirmed experimental trend.

Hydrogen crossover (HTO)

The predicted HTO value also varies nonlinearly with current density. It initially decreases as current density increases, then shows a slight increase at intermediate current density, followed by a further decrease at higher current density. Since HTO is estimated

using a semi-empirical correlation based on macroscopic operating parameters, this trend reflects the combined effects of current density, pressure, temperature, and proton transport assumptions in the model. The result indicates that hydrogen crossover is sensitive to operating conditions, but the exact quantitative trend would require further experimental validation for the specific POM-catalysed biomass electrolysis system.

5.1.2 Stack temperature (T_{stack})

The effect of stack temperature on the electrolysis performance was investigated in this section. Simulation results indicate that as Stack Temperature increases, the hydrogen production rate and Faraday efficiency increase, whereas the cell voltage and HTO decrease.

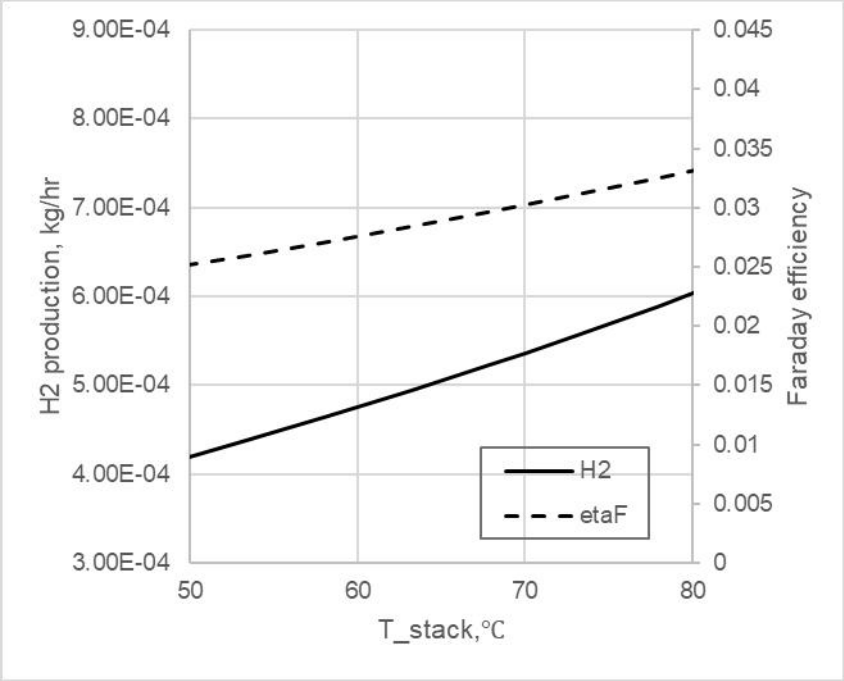

Figure 5.2. Model-predicted effect of stack temperature on H_2 production and Faraday efficiency

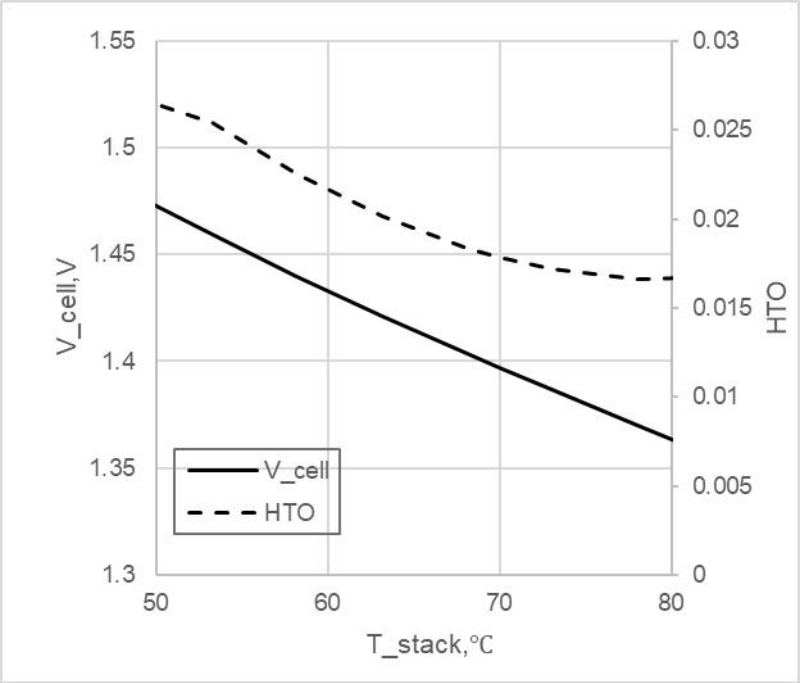

Figure 5.3. Model-predicted effect of stack temperature on cell voltage and hydrogen crossover

Higher temperature enhances ionic conductivity and electrode kinetics, reducing both activation and ohmic overpotentials, and thus lowering the required voltage. At the same time, faster reaction rates and improved mass transport promote more efficient hydrogen generation, increasing Faraday efficiency. Although gas diffusivity also rises with temperature, the enhanced mass transport and reduced local supersaturation limit crossover resulting in lower HTO.

5.1.3 Electric power input (W_{stack})

The effect of electric power input on the electrolysis performance was investigated in this section.

As electric power input increases, the cell voltage initially rises and then declines, while the current density increases monotonically. The HTO shows a non-monotonic response decreasing at first, then increasing for a period, and finally decreasing again. Hydrogen production exhibits a similar trend, rising sharply at low power, remaining nearly constant over a midrange, and increasing again at higher power inputs.

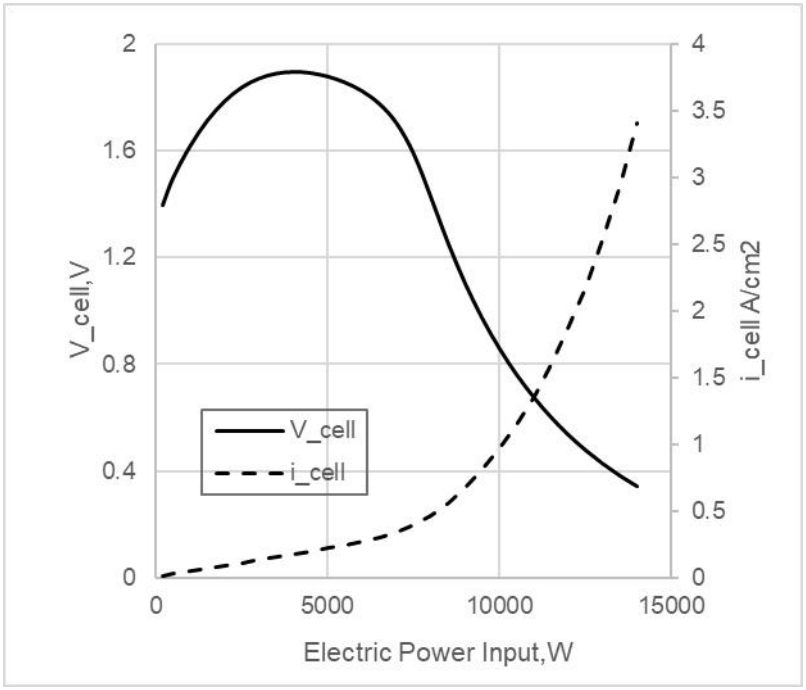

Figure 5.4. Model-predicted effect of electric power input on cell voltage and current density

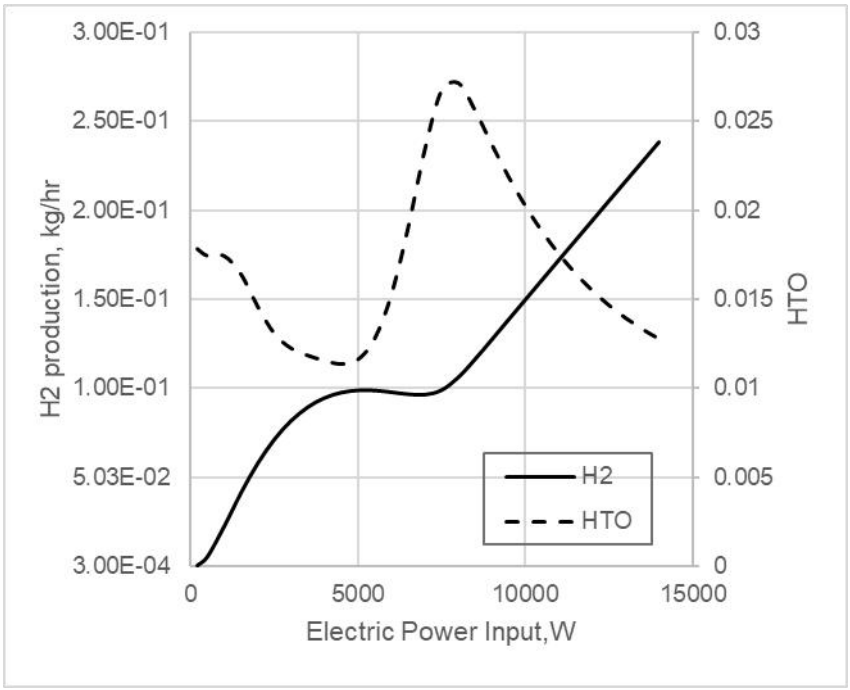

Figure 5.5. Model-predicted effect of electric power input on H_2 production and HTO

At low electric power input, the cell operates under the activation-controlled region, where the applied power primarily compensates for electrode overpotentials. The increase in power enhances reaction kinetics, raising both current density and hydrogen generation. Because the local temperature and ionic conductivity improve slightly in this regime, HTO

decreases due to enhanced separation efficiency.

As electric power input enters a midrange, cell voltage begins to decrease due to a shift from kinetic to ohmic limitation. The additional input power primarily contributes to overcoming electrolyte resistance rather than further accelerating the electrochemical reaction. The corresponding thermal and concentration gradients within the electrolyte may transiently enhance local gas diffusion, causing a modest increase in HTO and a temporary plateau in hydrogen output.

At higher electric power input, the system enters a diffusion-controlled region where both electrode reactions and gas removal processes are stabilized. The increased current density dominates energy utilization, leading to renewed growth in hydrogen production and a decline in HTO as mass-transfer constraints are alleviated. The observed nonlinearity reflects the intrinsic coupling between electrochemical overpotentials, ionic conductivity, and gas crossover behavior under varying electrical loading.

5.2 Steady-state simulation results

This section presents the results of the steady-state simulation and the preparation process for the dynamic model. The steady-state model provides the foundation for subsequent transient analysis by establishing consistent material and energy balances across all process units. Based on the steady-state simulation outputs, equipment sizing and operational boundaries were defined to ensure physical realism and numerical stability in dynamic simulation.

5.2.1 Steady-state results

The steady-state model was developed using Aspen Plus with a detailed representation of the electrolysis system by ACM and its auxiliary unit operations. The model includes the phosphoric acid electrolyser stack, flash tank, pump and heat-exchange units.

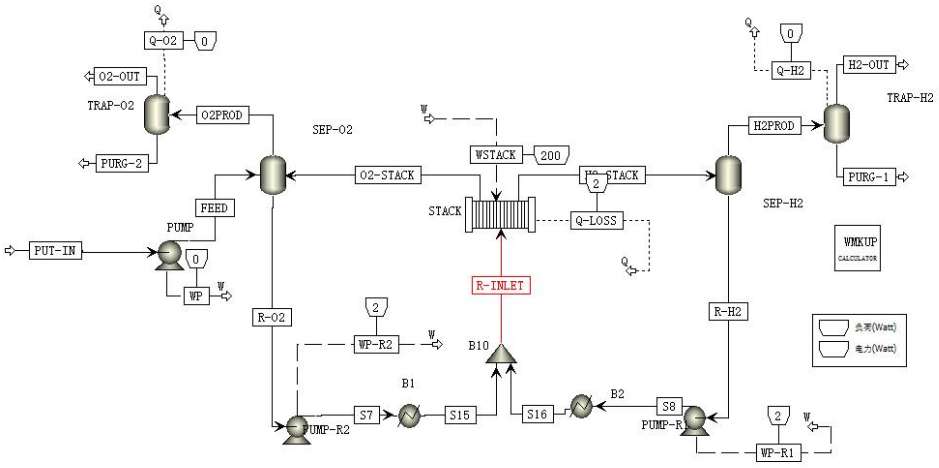

Figure 5.6. Aspen Plus flowsheet of the H_3PO_4-based POM-catalysed biomass electrolysis system

The overall material balance confirms stable hydrogen and oxygen generation consistent with Faraday's law, while the energy balance ensures that the stack temperature and heat exchange duties remain well-grounded. The steady-state model thus provides a physically reliable baseline for dynamic transition.

To further document the model-predicted steady-state stream results and provide the basis for subsequent analysis, the key stream results at steady state are summarized in Table 5.1.

Table 5.1 summarises the main electrolysis-related stream components used in the model, particularly those required for evaluating hydrogen production and hydrogen crossover into the anode-side oxygen-containing stream.

Table 5.1. Stream results

	PUT-IN	FEED	H2-STACK	O2-STACK
Temperature (℃)	25.00	25.47	75.07	75.06
Pressure (bar)	1.00	6.70	7.00	7.00
Vapor frac (molar)	0.00	0.00	0.00	0.00
Mass flows, (kg h^{-1})	5.53E-03	5.53E-03	2.97E+01	2.97E+01
H_2O	5.53E-03	5.53E-03	1.93E+01	1.93E+01
H_2	0	0	7.69E-04	4.91E-06
O_2	0	0	0	8.06E-03
H_3PO_4	0	0	1.04E+01	1.04E+01

	R-H2	R-O2	R-INLET
Temperature (℃)	75.07	75.05	72.01

Pressure (bar)	6.70	6.70	7.50
Vapor frac (molar)	0.00	0.00	0.00
Mass flows, (kg h^{-1})	2.97E+01	2.97E+01	5.94E+01
H_2O	1.93E+01	1.93E+01	3.86E+01
H_2	2.01E-04	2.01E-06	2.03E-04
O_2	0	3.53E-03	3.53E-03
H_3PO_4	1.04E+01	1.04E+01	2.08E+01

	H2PROD	H2-OUT	O2PROD	O2-OUT
Temperature (℃)	75.07	25.00	75.05	25.00
Pressure (bar)	6.70	1.00	6.70	1.00
Vapor frac (molar)	1.00	1.00	1.00	1.00
Mass flows, (kg h^{-1})	8.51E-04	7.35E-04	4.68E-03	4.62E-03
H_2O	2.82E-04	1.66E-04	1.43E-04	8.45E-05
H_2	5.69E-04	5.69E-04	2.90E-06	2.90E-06
O_2	0	0	4.54E-03	4.54E-03
H_3PO_4	5.80E-83	0	2.94E-83	0

This steady-state flowsheet establishes a reliable baseline for the system's operation, providing the necessary conditions and parameters for dynamic model preparation in future study. Key operating points, such as stack voltage, current, and flow rates, will serve as initial values for transient simulations

This preliminary work establishes a foundation for future, more comprehensive dynamic studies, which will include detailed equipment design, transient response analyses, and system optimization under variable operating conditions.

Table 5.2 summarises the major equipment sizing information used in the H_3PO_4-based POM-catalysed biomass electrolysis model. These values define the scale and configuration of the key unit operations in the Aspen Plus flowsheet and provide the basis for the subsequent steady-state performance analysis.

Table 5.2. Equipment sizing for major unit operations

	Stack	SEP-O2	SEP-H2	TRAP-O2	TRAP-H2
Inlet volume flow rate, cum/min	1.04E-03	5.30E-04	5.40E-04	1.09E-05	2.14E-05
Vapor Fraction, molar	0	1.23E-04	2.48E-04	1	1
Residence time, min	10	3	3	3	3
Safety factor	2	2	2	2	2
Volume of unit	2.07E-02	3.18E-03	3.24E-03	6.53E-05	1.29E-04
Length/diameter, m	0.44	0.15	0.15	0.05	0.06
Height, m	0.22	0.2	0.2	0.05	0.08
Width, m	0.22				

These preliminary sizing calculations provide a practical basis for the dynamic model. Detailed design and further optimization of all units under transient conditions will be addressed in future studies.

5.3 Performance analysis

In this section, the performance of the H_3PO_4 electrolyser system is analysed under different operating pressures. Five stack pressures were considered: 3, 5, 7, 9, and 11 bar. For each pressure, the electric power input to the stack was varied to observe its effect on key performance indicators, including hydrogen production rate, cell voltage, specific work, Faraday efficiency, and hydrogen crossover.

The objective of this analysis is to identify how pressure influences overall system efficiency, hydrogen purity, and energy consumption, while complementing the sensitivity analysis presented in section 5.1. Unlike Chapter 5.1, where single variables were systematically varied with controlled parameters, this chapter focuses on combined system-level performance under different operating pressures.

5.3.1 Specific work and HTO as a function of current density

The first analysis investigates the variation of specific work and HTO with current density (i_{cell}) under different stack pressures. The trends observed are:

Specific work rises sharply at low current density (~0–0.4 A/cm²), then gradually decreases beyond 0.4 A/cm². Specific work is insensitive to stack pressure.

HTO shows a similar trend initially, with a peak near current density≈ 0.4 A/cm². Unlike specific work, HTO is clearly influenced by pressure: higher pressures correspond to higher hydrogen crossover.

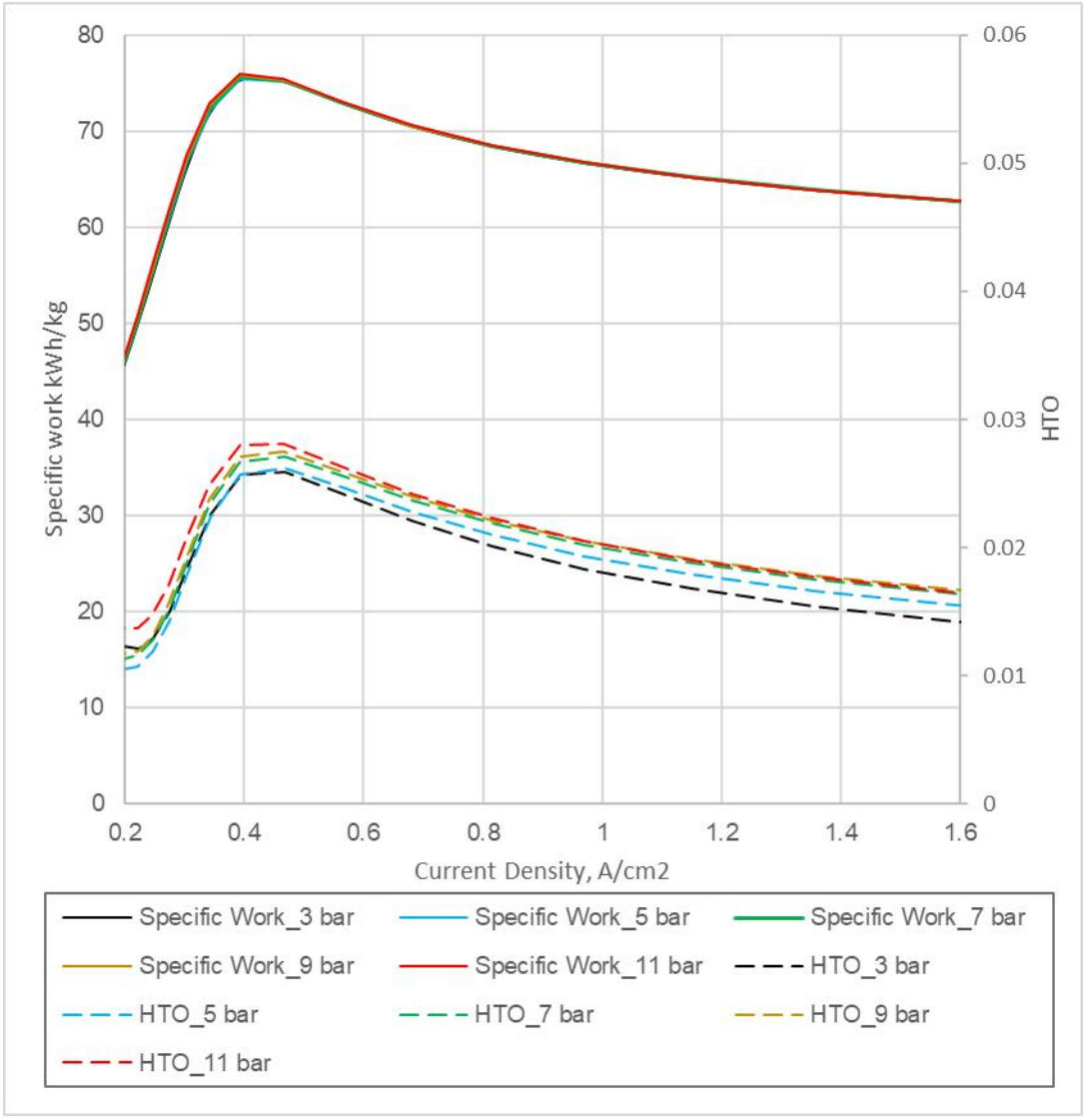

Figure 5.7. Current density vs. Specific work and HTO

The initial rapid rise in specific work corresponds to the activation-controlled regime, where the applied current strongly influences hydrogen generation. Beyond the intermediate current density, ohmic and mass transport limitations in the H_3PO_4 electrolyte moderate the incremental energy consumption per unit hydrogen, producing the observed decline in specific work. Elevated pressures enhance the solubility of hydrogen in the electrolyte and increase diffusion through the membrane, explaining the observed pressure-dependent increase in HTO.

5.3.2 Specific work and HTO as a function of hydrogen production

The second analysis examines specific work and HTO versus hydrogen production rate. Observations include:

Specific work initially decreases sharply at low hydrogen production, stabilizes across intermediate production levels, then rises slightly when hydrogen output decreases. The resulting curve resembles a skewed "U." Stack pressure has minimal effect on specific work.

HTO decreases initially, then rises in the mid-range, forming a roughly triangular profile, before decreasing again. Pressure has a complex effect: before the lowest HTO point, lowest and highest pressures correspond to higher HTO, while after the minimum, higher pressures yield larger HTO values.

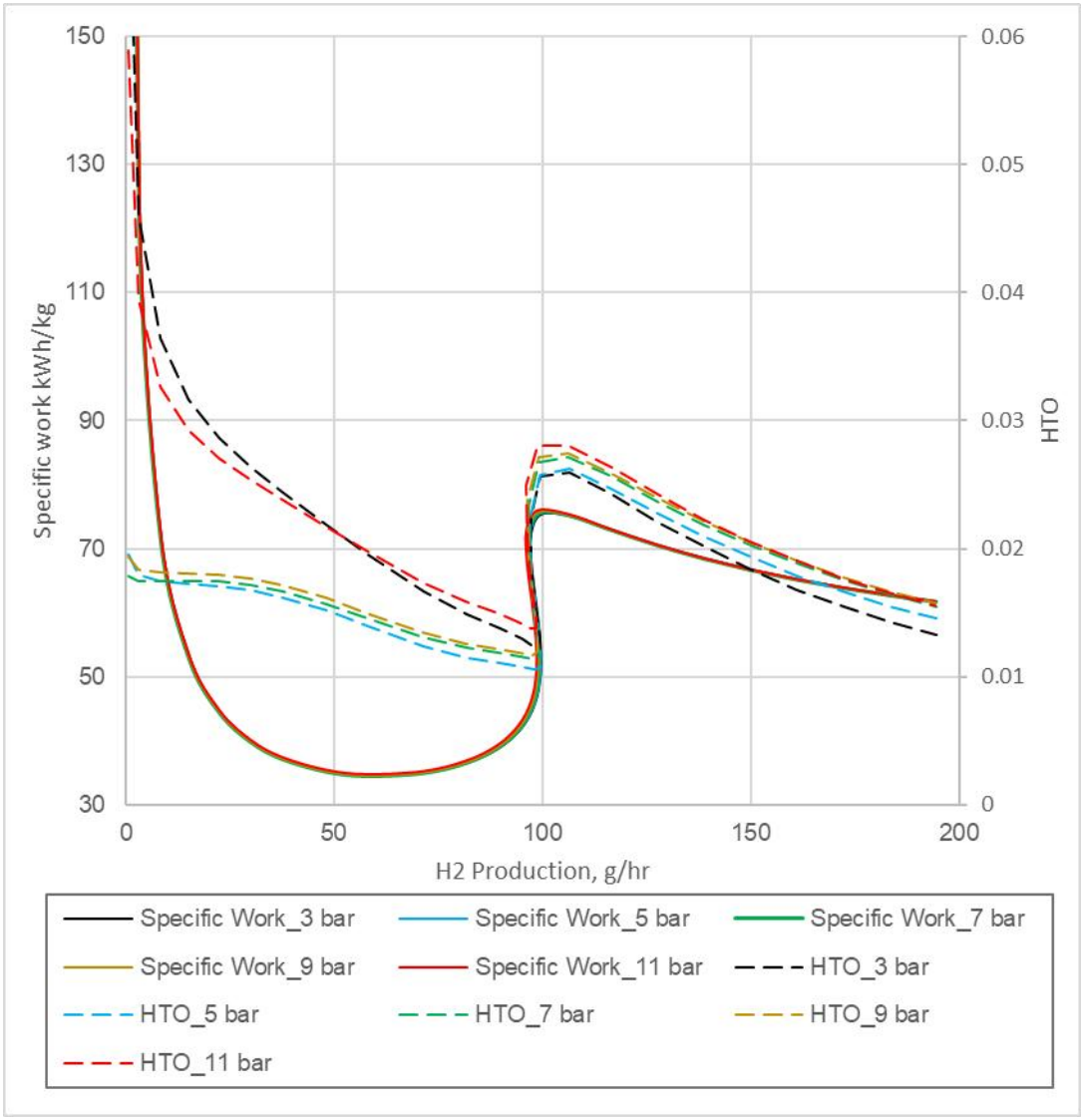

Figure 5.8. Hydrogen production vs. Specific work and HTO

The non-monotonic behavior of H_2 and specific work can be attributed to limitations in mass transport and ionic conductivity. As electric power input increases, the stack drives higher current density, enhancing hydrogen production. Once transport limits are approached, additional power does not proportionally increase H_2 generation, temporarily lowering hydrogen flow while increasing energy consumption, resulting in a sharp rise in specific work. HTO behavior reflects the balance between hydrogen flux, crossover through the membrane, and local diffusion effects.

5.3.3 Specific work and Faraday efficiency as a function of hydrogen production

The third analysis focuses on Faraday Efficiency and specific work versus hydrogen production:

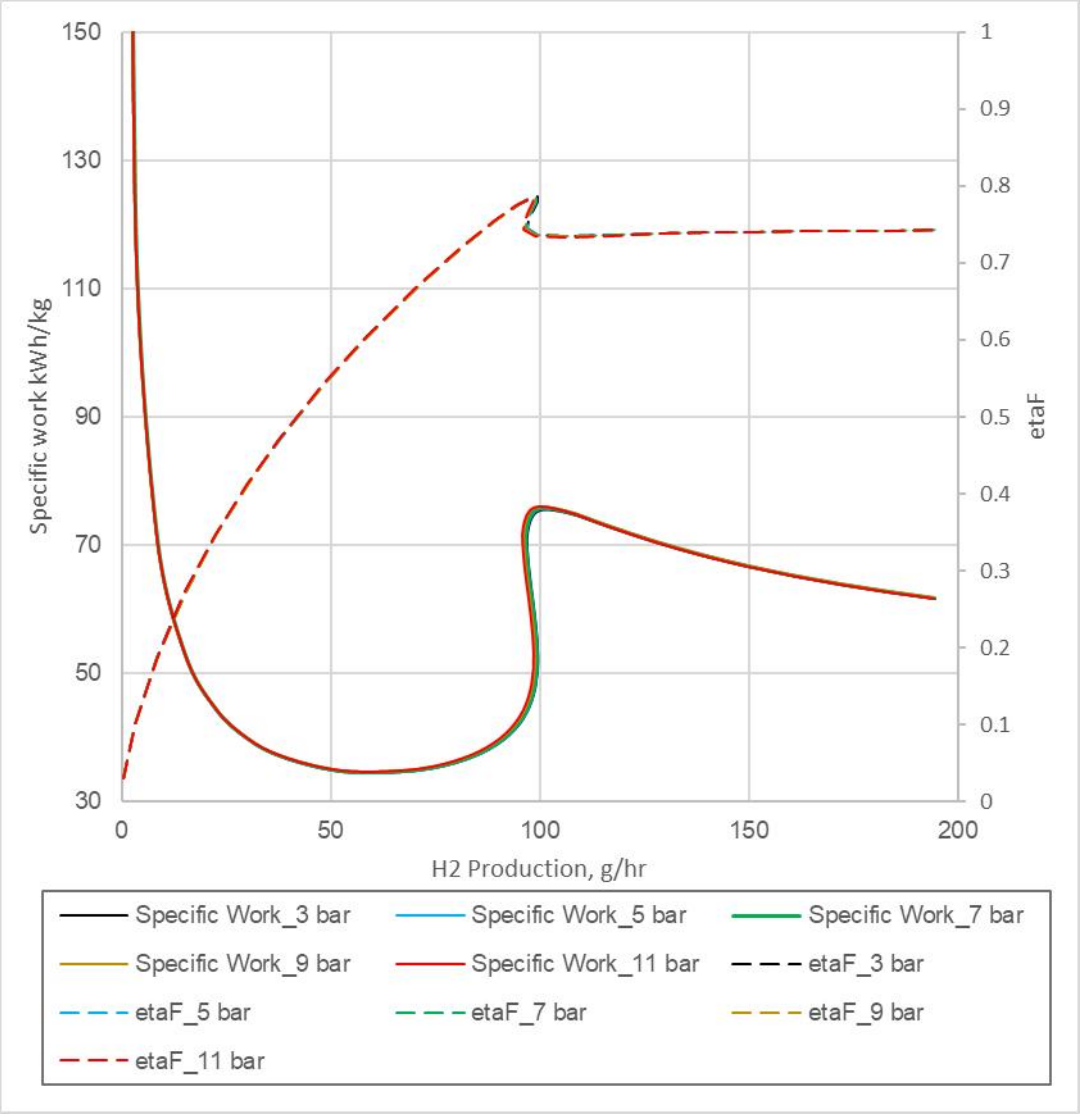

Figure 5.9. Hydrogen production vs. Specific work and Faraday Efficiency

The third analysis examines the relationship between hydrogen production, specific work, and Faraday efficiency. As shown in Figure 5.9, the variation of specific work follows the same general trend discussed in the previous sections, indicating that energy consumption remains closely related to hydrogen production rate. The model-predicted Faraday efficiency initially increases with hydrogen production, reaches a local maximum, then decreases slightly before showing a gradual secondary increase. This behaviour may reflect the combined influence of electrochemical reaction rate, hydrogen crossover, and transport-related losses considered in the semi-empirical model [77, 79]. Within the pressure range investigated in this study, stack pressure has only a limited influence on Faraday efficiency, suggesting that current density and hydrogen crossover assumptions play a more dominant role in the predicted Faraday efficiency trend.

5.3.4 Summary

The sensitivity analysis under different stack pressures (3, 5, 7, 9, 11 bar) reveals several key trends in hydrogen production, HTO, specific work, and Faraday efficiency. The specific work exhibits a non-linear, U-shaped dependence on both current density and hydrogen production. At low current densities or low electric power input, activation-controlled kinetics dominate, leading to relatively high energy input per mole of hydrogen. As the electrochemical flux increases, the specific work decreases sharply and enters a plateau region, reflecting improved electron utilization and temporary mitigation of transport limitations. At higher hydrogen production, localized diffusion and crossover effects contribute to a moderate rise in specific work, followed by partial stabilization as the system approaches higher flux conditions. Notably, stack pressure has minimal influence on specific work, indicating that internal electrochemical and transport processes primarily govern energy efficiency.

HTO exhibits a complex dependence on stack pressure and operating conditions. For the first plot versus current density, HTO increases with higher stack pressure: at identical current density values, higher pressure curves consistently shows higher HTO than lower pressure curves, indicating that elevated pressure promotes hydrogen permeation into the oxygen stream. For the second plot versus hydrogen production, HTO displays a non-monotonic trend:

before the minimum point in HTO, the 3 bar case shows the largest HTO, followed by 11 bar and intermediate pressures; after the minimum, higher pressures result in higher HTO. This indicates that both very low and very high pressures are unfavorable for minimizing hydrogen crossover, while moderate pressures achieve a better balance between efficient hydrogen generation and controlled HTO.

Faraday efficiency generally increases with hydrogen production initially, reaches a peak, then slightly decreases before partially recovering. This reflects the balance between electron utilization for hydrogen generation and temporary limitations due to transport and crossover effects.

From a practical standpoint, the preferred operating region balances low specific work, high Faraday efficiency, and minimized HTO. This is typically achieved at moderate electric power input and intermediate hydrogen production rates, where activation losses are reduced, transport limitations are manageable, and hydrogen crossover is limited. These findings provide guidance for optimizing operational strategies and inform design considerations for future studies.

The study utilized Aspen Plus and Aspen Custom Modeler to simulate the process and analysed key performance indicators under different operating conditions.

Key findings from the research emphasize the direct correlation between power input and hydrogen volumetric flow rate, with data in Table 5.1 and Figure 5.1 indicating a notable increase in flow rate from about 0.1498 m^3/hr at 1 kW to approximately 1.0921 m^3/hr at 6 kW. Further analysis of hydrogen production efficiency reveals a reduction in specific work as production rates increase, as depicted in Table 5.2 and Figure 5.2; for instance, the specific work drops from 138.24 kWh/kg for a production rate of 3.62 g/hr to 41.73 kWh/kg for a rate of 119.81 g/hr, signifying higher efficiency at elevated production levels. Steady-state simulation outcomes are consistent with expectations, substantiating the viability and dependability of the models developed for PEM water electrolysis and POM catalyst biomass electrolysis, which adeptly represent the systems' dynamic responses to varying operational parameters and their influences on hydrogen production rate and efficiency. The operational efficiency analysis underscores the capacity of both electrolysis methods to attain high

efficiency under optimal conditions, with a marked increase in hydrogen production rate accompanying higher power inputs and a decrease in the specific work needed for hydrogen production as the rate escalates, showcasing the scalable and efficient potential of these hydrogen production processes.

The dynamic response analysis provides a comprehensive understanding of the performance characteristics of biomass electrolysis using POM catalysts. The results show that this approach can achieve high efficiency and high hydrogen production rates under optimal conditions. The literature-supported model provides a powerful framework for further optimization and scaling up of these technologies towards practical large-scale hydrogen production.

PEM water electrolysis, an electrochemical process that employs a proton exchange membrane to split water into hydrogen and oxygen, is lauded for its high efficiency, quick response times, compact design, and moderate operating temperatures, yet faces economic challenges primarily due to the cost of catalysts like platinum. Economically, PEM electrolysis excels in efficiency for small-scale applications but may be hindered by its cost implications. In contrast, biomass electrolysis, catalysed by polyacid tungstate (POM), capitalizes on renewable biomass resources for hydrogen production, offering the benefits of low-cost catalysts and minimizing the reliance on precious metals, yet it grapples with technical and commercialization challenges along the biomass supply chain, catalyst development, and system design. A comparative economic analysis must consider a spectrum of factors including raw material, catalyst, equipment costs, energy efficiency, and operational expenses, where PEM electrolysis might be at a disadvantage due to catalyst costs but could be competitive in high-efficiency applications, while biomass electrolysis with POM catalysts may have a catalyst cost edge but must navigate the complexities of technological advancement and biomass supply economics.

5.4 Comparative analysis: PEM water electrolysis vs. POM-catalysed biomass electrolysis

In order to evaluate the electrochemical behavior of biomass electrolysis systems relative to traditional water electrolysis, three key performance indicators were compared under the same stack configuration: (1) specific power and hydrogen production rate, (2) battery voltage and current density, and (3) hydrogen production and power input. The impact of acidic H in the catalyst electrolyte is highlighted in relation to energy efficiency, reaction kinetics, and gas evolution characteristics, as compared to neutral H ₂ O.

Specific work vs. Hydrogen production

In the pure-water system, the specific work increases monotonically with hydrogen production: it rises sharply at low H_2 generation rates, then continues to increase gradually. This trend is typical for neutral electrolytes, where higher current densities lead to increasing ohmic and activation losses, resulting in greater energy consumption per unit of hydrogen.

In contrast, biomass electrolysis systems exhibit obvious multi-stage behavior. At low hydrogen production rates, the specific power is initially very high, then rapidly decreases to a stable low region, then increases again at higher loads, and finally shows a slight decrease. The initial high value reflects the activation dominated state in acidic electrolytes, where protons transfer through viscous H to the substrate and slow electrode kinetics require an increase in overpotential. As the reaction progresses, the ion conductivity increases with the rise of temperature and proton mobility, leading to a decrease in mid-range specific work. At very high-power inputs, mass transfer and bubble resistance dominate, once again increasing energy demand.

Overall, once a stable proton conduction is established in the biomass electrolysis system, its performance is superior to pure water in most operating ranges, confirming its advantage as a conductive electrolyte that can reduce overall energy intensity during continuous operation.

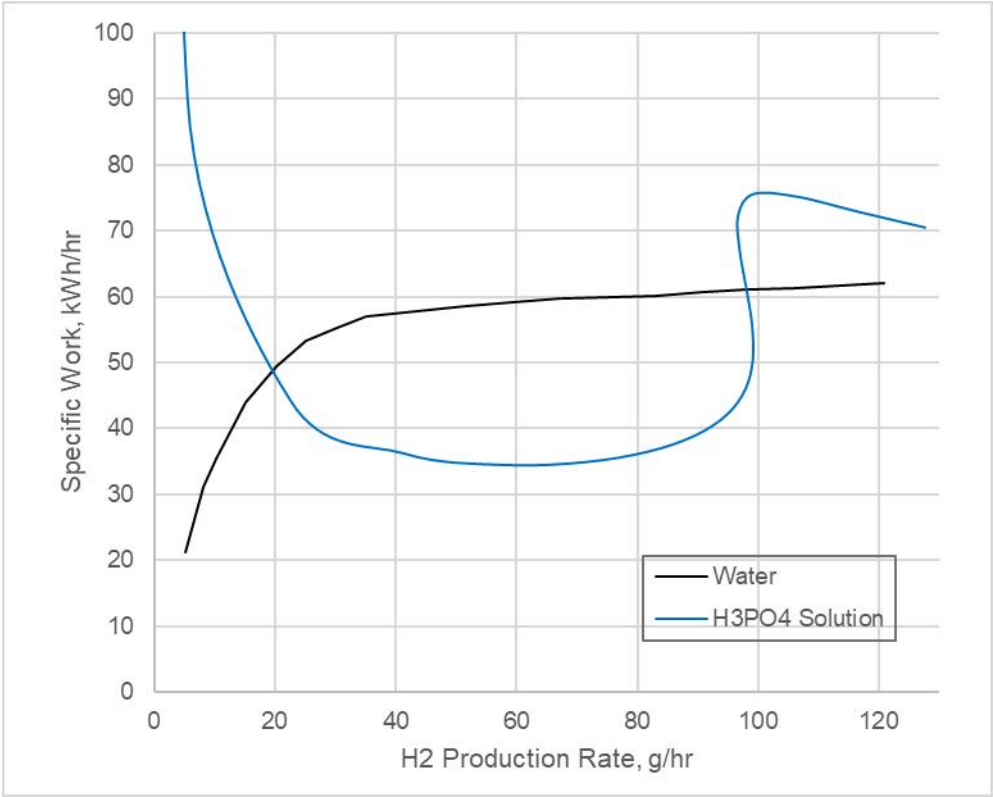

Figure 5.10. Specific work vs. Hydrogen production

Cell voltage vs. Current density

For pure water, the cell voltage increases sharply with current density at low i_{cell}, then flattens at higher loads — consistent with classical polarization behavior where activation losses dominate initially and ohmic effects govern thereafter.

On the contrary, biomass electrolysis shows a brief initial increase with the increase of i-batteries, followed by a gradual decrease in voltage. The brief initial increase corresponds to the activation polarization region, followed by enhanced proton conduction in the acidic electrolyte, which reduces the effective overpotential. Once the proton pathway is fully established, improved charge transfer and lower ion resistance can be maintained at lower voltages than pure water.

It is worth noting that the voltage of biomass batteries is always lower than that of water

outside the low current region, which confirms that acid helps with ion transport and reduces the total polarization resistance.

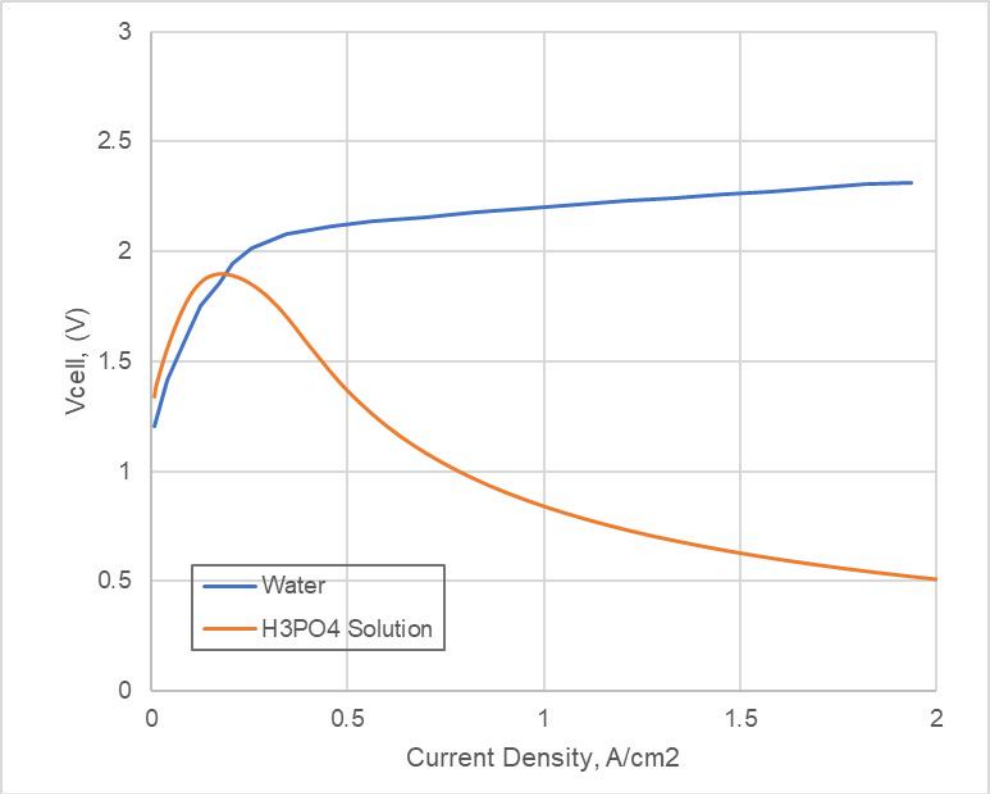

Figure 5.11. Cell voltage vs. Current density

Hydrogen Production vs. Stack Power Input

In both systems, as expected by Faraday's law, hydrogen production increases with increasing power input to the fuel cell stack. However, although pure water initially produces more hydrogen at low power due to its lower conductivity loss at minimum load, biomass electrolysis systems surpass it with increasing power input. The observed trend suggests that effective proton conduction is activated in acidic media, where an increase in ion mobility and minimization of electrode overpotential result in a higher rate of H evolution with equal force.

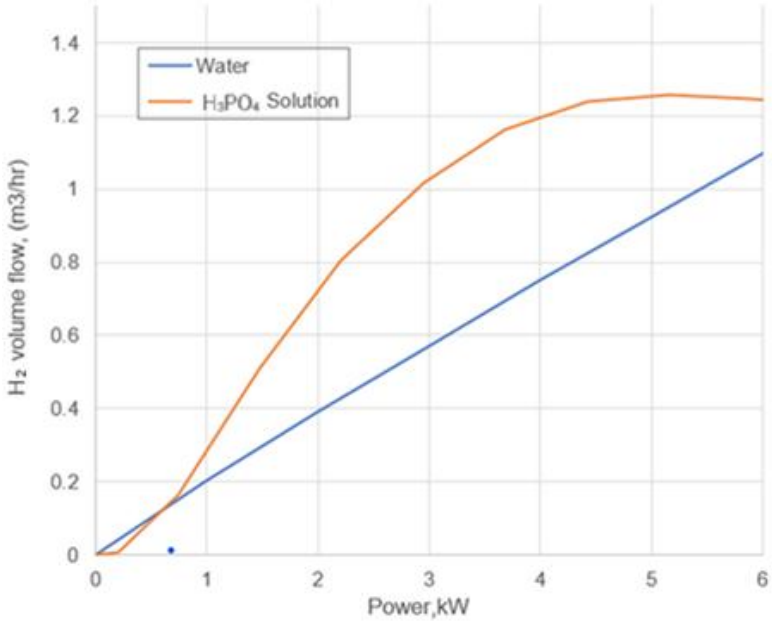

Figure 5.12. Hydrogen production vs. Stack power input

Overall, comparisons indicate that biomass electrolysis initially requires higher energy input due to slow activation kinetics, but once the electrolyte stabilizes thermally and electrochemically, it quickly becomes more efficient.

Chapter 6: Comparative economic analysis

The comparative performance analysis in Chapter 5 indicated that the POM-catalysed biomass electrolysis system operates at a significantly lower specific work (energy consumption) than traditional PEM water electrolysis. This chapter builds on these findings by first calculating the electricity-cost contribution, which represents the main operating cost considered in this study, and then discussing capital and other cost factors with reference to the literature.

This chapter provides a preliminary economic comparison of PEM water electrolysis and POM-catalysed biomass electrolysis. Section 6.1 presents the main simulation-derived electricity-cost analysis based on the calculated specific work and the assumed electricity price. The subsequent sections place these results in a broader economic context by discussing capital cost, operating cost, hydrogen production cost, energy-related performance, and technology maturity using literature-based data and qualitative comparison. In this way, the chapter provides an initial techno-economic interpretation of the two routes, while a complete project-level LCOH assessment is identified as a topic for future work.

6.1 Simulation-based electricity cost analysis

The dominant operating expenditure (OPEX) for any electrolysis system is the cost of electricity. A simplified, direct economic comparison can be made by calculating the electricity cost per kilogram of hydrogen (H_2) produced. This cost is calculated based on the specific work (energy consumption) derived from this study's simulation results (presented in Section 5.5, Figure 5.10) and an assumed industrial electricity price. The governing equation is:

$$\text{Electricity Cost}\left(\frac{\$}{\text{kg H2}}\right) = \text{Specific Work}\left(\frac{\text{kWh}}{\text{kg H2}}\right) \times \text{Electricity Price}\left(\frac{\$}{\text{kWh}}\right) \quad (6.1)$$

For this analysis, an industrial electricity price of \$0.10 per kWh is assumed. This is a conservative estimate, as recent data from the U.S. Energy Information Administration (EIA) show that the average industrial electricity prices in the United States were 8.13 cents/kWh in 2024 and 8.62 cents/kWh in 2025 [80]. In comparison, the International Energy Agency

reported that electricity prices for energy-intensive industries in the European Union remained more than twice the U.S. level in 2025 [81].

The calculated electricity cost as a function of the H_2 production rate for both the PEM and POM systems is presented in Figure 6.1. This plot is a direct economic translation of the specific work data from Figure 5.10.

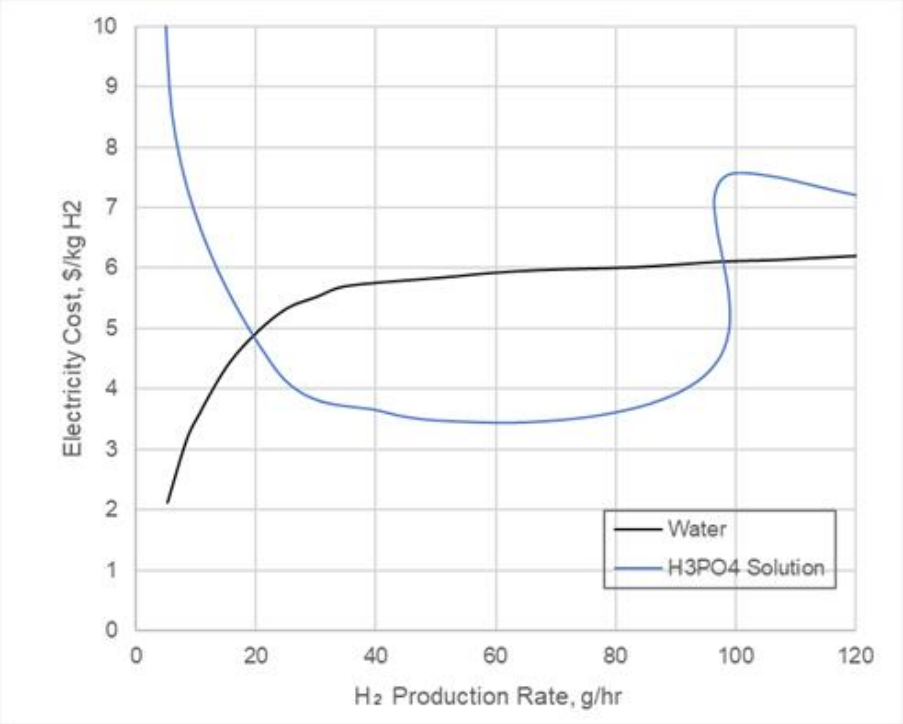

Figure 6.1. Calculated electricity cost vs. H_2 production rate for PEM and POM systems

Figure 6.1 directly visualizes the economic implications of the two simulated technologies. The plot shows several key trends:

PEM water electrolysis: The electricity cost for the PEM system rises as production begins and then increases more gradually, stabilizing around \$6.00 per kg H_2 across the typical operating range (e.g., 80 g/hr).

POM-catalysed biomass electrolysis: The POM exhibits a much different profile. The cost is extremely high at very low production rates, but it then plummets as the system overcomes initial activation barriers. The cost then stabilizes in a wide low-cost operating region at approximately \$3.50 per kg H_2.

Figure 6.1 shows a lower model-predicted electricity-cost contribution for the POM-catalysed biomass electrolysis system compared with the PEM water electrolysis

system under the simulated steady-state conditions. At a stable production rate of 80 g/hr, the biomass system's electricity cost ($3.50/kg H_2) is approximately 41.7% lower than the PEM system's cost ($6.00/kg H_2). This cost saving is a direct result of the more favorable thermodynamics of the POM-catalysed reaction, which allows the system to operate at a much lower cell voltage for a given current density. While this analysis does not include capital costs, it provides a direct, simulation-based validation of the primary economic potential of the POM-catalysed biomass electrolysis route.

6.2 Capital cost

The initial *capital* cost (CAPEX) is also a critical factor in a project's feasibility. This section provides a high-level, qualitative comparison of the key capital cost components for both systems, based on literature [48].

Table 6.1. Capital cost component comparison.

Project	PEM water electrolysis	POM-catalysed biomass electrolysis
Electrolytic cell material	Expensive (titanium, precious metal catalysts such as platinum/iridium)	Can be lower (conventional electrode + POM as catalyst)
System composition	Highly modular, suitable for scalability	The system structure is complex and involves organic matter treatment
Total equipment investment	High	Medium low

6.3 Operating cost

Beyond the electricity cost analysed in Section 6.1, other operating expenditures (OPEX) must be considered, such as maintenance and consumable materials. The POM-catalysed system introduces different operational factors, like catalyst regeneration, which are compared to the established PEM system in Table 6.2 [48].

Table 6.2. Qualitative operating cost comparison.

Project	PEM water electrolysis	POM-catalysed biomass electrolysis
Catalyst replacement frequency	Medium (durability of precious metal catalysts)	POM catalyst soluble recycling regeneration with low operating costs
Operational complexity	Low to moderate level of automation	Medium, involving raw material pretreatment and product separation

6.4 Hydrogen production cost context

Section 6.1 presents the simulation-derived electricity-cost contribution for hydrogen production. Based on the calculated specific work and the assumed electricity price of \$0.10/kWh, the electricity-related production cost is approximately \$6.00/kg H_2 for PEM water electrolysis and approximately \$3.50/kg H_2 for POM-catalysed biomass electrolysis under the representative operating region. These results suggest that the POM-catalysed biomass electrolysis route may reduce the electricity-related part of hydrogen production cost by lowering the anodic energy requirement.

However, total hydrogen production cost is also affected by capital investment, stack lifetime, maintenance, catalyst cost, feedstock supply, product separation, and other operating factors. Therefore, the values calculated in Section 6.1 are used here as electricity-cost indicators rather than complete LCOH values. Previous techno-economic studies have shown that the full cost of water electrolysis is strongly influenced by electricity price, electrolyser capital cost, system configuration, and operating assumptions [48]. For POM-catalysed biomass electrolysis, complete LCOH data are still limited because the technology remains at an earlier research stage. Its full economic performance would depend on biomass feedstock availability, POM catalyst recovery, product separation, and long-term stability.

Therefore, the main quantitative economic result of this thesis is the electricity-cost comparison. A complete LCOH assessment for POM-catalysed biomass electrolysis is

recommended as future work.

Table 6.3. Hydrogen production cost context and literature-based comparison

Project	PEM water electrolysis	POM-catalysed biomass electrolysis
Simulation-derived electricity-cost contribution in this study	Approximately $6.00/kg H_2	Approximately $3.50/kg H_2
Literature-based full-cost context	Strongly affected by electricity price, electrolyser CAPEX, system configuration, and stack lifetime [48]	Full LCOH benchmark is not yet well established.
Cost stability	Highly dependent on electricity price and equipment lifetime	Potentially lower electricity-cost contribution, but higher uncertainty in feedstock handling and catalyst recycling

6.5 Energy efficiency

Energy efficiency is an important factor in comparing PEM water electrolysis and POM-catalysed biomass electrolysis. In this study, the comparison is mainly based on the simulation-derived specific work and electricity-cost results discussed in Section 6.1. Since electricity consumption is a major contributor to hydrogen production cost, lower specific work indicates more favourable energy-related performance.

For PEM water electrolysis, energy demand is mainly associated with water splitting, activation overpotential, ohmic resistance, and mass-transfer losses. The anodic oxygen evolution reaction is kinetically slow and contributes significantly to the required cell voltage. In contrast, POM-catalysed biomass electrolysis uses biomass oxidation to replace or partially avoid the oxygen evolution reaction. In this process, biomass acts as an oxidisable feedstock, while POM functions as a redox mediator under acidic conditions. This mechanism can reduce the anodic energy requirement and lower the electricity input for hydrogen production.

The simulation results show that POM-catalysed biomass electrolysis has lower specific work and a lower electricity-cost contribution than PEM water electrolysis under the representative operating region. This trend is consistent with recent experimental studies on POM-catalysed biomass electrolysis, which reported lower electricity-use potential for

selected biomass and food-waste feedstocks compared with conventional water electrolysis [83]. However, the overall energy performance of this route also depends on biomass preparation, POM recovery, product separation, and long-term operation.

Table 6.4. Energy efficiency and by-product comparison.

Project	PEM water electrolysis	POM-catalysed biomass electrolysis
Main reaction route	Water splitting with oxygen evolution	Biomass-assisted electrolysis with POM-mediated oxidation
Energy demand	Electricity for water splitting and cell losses	Lower electricity input assisted by biomass oxidation
Simulation result	Higher specific work	Lower specific work
By-products	Oxygen	Oxidised biomass-derived products
Main uncertainty	Electricity price, stack efficiency, degradation	Biomass variability, POM recovery, separation, long-term stability

Overall, POM-catalysed biomass electrolysis shows promising electricity-saving potential, but a complete process-level energy assessment would require further analysis of biomass handling, catalyst recovery, separation, and scale-up operation.

6.6 Technology maturity and development risk

Technology maturity is an important factor in evaluating the practical feasibility of hydrogen production routes. PEM water electrolysis is already commercially available and has been widely studied for renewable hydrogen production. It benefits from high hydrogen purity, compact system design, fast dynamic response, and good compatibility with intermittent renewable electricity. However, its wider deployment is still affected by high electricity demand, expensive membrane materials, noble metal catalysts, and stack lifetime.

POM-catalysed biomass electrolysis is at an earlier stage of development. Recent studies have demonstrated its potential for hydrogen production from biomass components and food-waste feedstocks, with POM acting as a redox mediator under acidic conditions [82]. This route may reduce the anodic energy requirement by replacing or partially avoiding the oxygen evolution reaction. However, further development is still required in biomass feedstock handling, POM recovery and recycling, product separation, long-term stability, and scale-up design.

Table 6.5. Technology maturity and risk comparison.

Project	PEM water electrolysis	POM-catalysed biomass electrolysis
Technology status	Commercially available and widely studied	Laboratory-scale / early-stage research
Main strength	High H_2 purity, fast response, compact design, renewable-power compatibility	Potential reduction in anodic energy demand through biomass oxidation
Main limitation	High electricity demand, expensive catalysts and membranes, stack degradation	Biomass variability, POM recovery, separation, long-term stability
Cost data availability	Supported by established techno-economic literature	Full cost data are still less established
Development risk	Lower technical risk but higher cost pressure	Higher scale-up uncertainty but promising electricity-saving potential

6.7 Summary of economic assessment

This chapter provided a preliminary economic comparison between PEM water electrolysis and POM-catalysed biomass electrolysis. The main quantitative result is the simulation-derived electricity-cost contribution based on the calculated specific work and the assumed electricity price of \$0.10/kWh. Under the representative operating region, the electricity-related cost was approximately \$6.00/kg H_2 for PEM water electrolysis and approximately \$3.50/kg H_2 for POM-catalysed biomass electrolysis. This indicates that the POM-catalysed biomass electrolysis route may reduce the electricity-related part of hydrogen production cost by lowering the anodic energy requirement through biomass oxidation.

The broader economic discussion shows that PEM water electrolysis has a more established cost and technology basis, but it remains strongly affected by electricity price, electrolyser capital cost, noble metal catalysts, membrane durability, and stack lifetime. In contrast, POM-catalysed biomass electrolysis shows promising electricity-saving potential, but its full economic performance depends on biomass feedstock supply, POM catalyst recovery, product separation, long-term stability, and scale-up feasibility.

Overall, the results suggest that POM-catalysed biomass electrolysis has potential advantages in electricity-related cost and energy performance. However, its complete LCOH

and commercial feasibility require further investigation through detailed process design, catalyst recycling analysis, long-term operation data, and full techno-economic assessment.

Chapter 7: Outlook

7.1 Outlook for future research

This study's simulation results demonstrate the theoretical potential of POM-catalysed biomass electrolysis for improving energy efficiency and reducing costs compared to traditional PEM water electrolysis. Building upon the steady-state models developed in this work, future research should focus on the following key areas:

Dynamic Simulation and Process Control: This study was limited to steady-state analysis for the biomass system. The critical next step is to develop a full dynamic simulation of the POM-catalysed process. This would be important for analysing transient behaviour, start-up and shutdown procedures, and system performance under intermittent renewable electricity inputs such as solar and wind power.

Catalyst Stability and Lifetime Modelling: The current model assumes stable catalyst performance. A key unknown in real-world applications is the long-term stability of the POM catalyst under continuous operation. Future research should investigate catalyst degradation mechanisms and incorporate these lifetime models into the simulation to assess long-term economic viability.

Techno-Economic Scale-Up: Building on the preliminary economic analysis in Chapter 6, a full-scale process design and techno-economic assessment is required. This would involve designing efficient biomass pretreatment systems, catalyst recovery and regeneration loops, and a reliable biomass supply chain to evaluate the commercial feasibility of this technology.

7.2 Conclusion

This thesis presented a comparative simulation study of hydrogen production via PEM water electrolysis and POM-catalysed biomass electrolysis. The novelty of this work lies in developing a process-level Aspen Plus and Aspen Custom Modeler framework to compare a conventional PEM water electrolysis route with POM-catalysed biomass electrolysis route under a consistent modelling basis. The main findings are summarized as follows:

Simulation Model Development: A modified Aspen Custom Modeler (ACM) framework was developed for the POM-catalysed biomass electrolysis system by adapting a standard PEM electrolysis model. The resulting model provides a process-level representation of the H_3PO_4-based POM-mediated biomass electrolysis pathway.

Performance and Efficiency: The model-predicted results indicate that POM-catalysed biomass electrolysis can operate at lower cell voltage and lower specific work than PEM water electrolysis under the assumptions and representative operating conditions used in this study.

Economic Potential: The steady-state analysis projects that the POM-catalysed biomass electrolysis system's electricity cost could be over 40% lower than the PEM system's, highlighting its strong economic potential.

Foundation for Future Work: This work provides a solid modelling foundation and a literature-supported steady-state baseline for the future development of biomass electrolysis technology, contributing valuable insights to the advancement of green hydrogen production.

Appendix

Implementation of Aspen Plus Stack Module

The Aspen Plus Stack module used in this study was developed and installed to enable process-level representation of the electrochemical behaviour of the electrolyser unit. The following steps summarize the implementation procedure.

First, the customized Stack model package (*Stack1.atmlz*) was obtained from Aspen Custom Modeler (ACM). This file contains the compiled electrochemical subroutines necessary to represent current density–voltage characteristics, cell temperature response, and Faraday efficiency within electrolyser unit. To integrate the model, the *Stack1.atmlz* file was double-clicked and executed, automatically installing the module into the Aspen Plus model library. After installation, the Stack component became accessible from the Aspen Plus unit operation palette under the "User Models" section.

Next, the main simulation file (*KOH_V12.apwz*) was developed by Aspen Plus. This file includes the process flowsheet representing the overall electrolysis system. The Stack module was inserted into the process flow,

After specification of all necessary inputs, the model was fully configured and ready for simulation. This setup enabled subsequent study of PEM and biomass-assisted electrolysis processes described in Chapter 3.

Structure and Formulation of the ACM Stack Model

The stack model implemented in this study derives from the modular ACM implementation originally proposed by Sánchez and later adapted by Humbird. The implemented ACM component exposes standard I/O ports—INLET (mole-fraction feed port), OUTcathode and OUTanode (product ports), a work port WSTACK and a heat port QLOSS—permitting direct embedding into the Aspen Plus process flowsheet.

Model configuration: principal user parameters are P_{stack} (stack pressure, bar), N_{cell} (number of cells) and A_{cell} (active cell area, m²). Numerous hidden realparameters capture empirical physics (resistive terms r1–r2, pressure/temperature dependences d1–d2,

activation-fit coefficients s, t1–t3, Faradaic regression constants f11–f22, and HTO/transport coefficients C1–C9, E1–E9). A constant reversible voltage Vrev is defined for baseline thermodynamics.

Governing relations: six principal equations (EQ_1–EQ_6) determine stack behaviour. EQ_1 is a semi-empirical V_{cell} relation combining Vrev, ohmic/resistive terms and a logarithmic activation term. EQ_2 parameterizes Faraday efficiency ηF as a function of current density and temperature. EQ_3 computes hydrogen crossover (HTO) as a temperature/pressure/current dependent empirical expression. EQ_4 enforces the electrical power balance ($W_{stack} \leftrightarrow V_{cell} \cdot i_{cell} \cdot N_{cell} \cdot A_{cell}$). EQ_5 converts ηF and i_{cell} to reaction extent (mol) via Faraday's law, with an additional empirical scaling in this implementation to match H_3PO_4 behavior. EQ_6 specifies a proportional ambient heat loss (Q_{loss}) tied to reaction enthalpy.

Mass and energy closure are checked internally: aaMBzero (mass balance residual) and aaHBone (energy balance ratio) provide diagnostic flags. Thermophysical properties (enthalpy, density) are called via Aspen property functions for outlet composition and temperature coupling. After all required inputs and boundary conditions were specified and component links configured, the compiled module (Stack1.atmlz) was installed through the Aspen User Model Manager and connected to the flowsheet. Successful execution and acceptable mass/energy residuals confirmed correct integration and readiness for parametric simulation.

Electrolysis Cell Stack Model Description

The electrolysis cell stack module (STACK) simulates the generation of hydrogen and oxygen under steady-state conditions. The production rates of both gases are governed by the stack's operating temperature, pressure, and electrical power input. The cell stack is modeled as operating under adiabatic conditions, except for a defined fraction of heat loss to the surroundings. The remaining reaction energy is distributed to the outlet streams, resulting in a moderate temperature increase. Hydrogen is evolved at the cathode outlet and oxygen at the anode outlet. The model assumes equal operating pressure on both the anode and cathode

sides to ensure a balanced electrolyte flow. The produced gas mixtures are subsequently separated via a flash separation process.

References

[1] Zou, C., Li, J., Zhang, X., Jin, X., Xiong, B., Yu, H., et al. (2022). Industrial status, technological progress, challenges, and prospects of hydrogen energy. Natural Gas Industry B, 9(5), 427-447. https://doi.org/10.1016/j.ngib.2022.04.006

[2] Rolo, I., Costa, V. A., & Brito, F. P. (2023). Hydrogen-Based Energy Systems: Current Technology Development Status, Opportunities and Challenges. Energies, 17(1), 180. https://doi.org/10.3390/en17010180

[3] Sarker, A. K., Azad, A. K., Rasul, M. G., & Doppalapudi, A. T. (2023). Prospect of green hydrogen generation from hybrid renewable energy sources: A review. Energies, 16(3), 1556. https://doi.org/10.3390/en16031556

[4] Zhang, B., Zhang, S. X., Yao, R., Wu, Y. H., & Qiu, J. S. (2021). Progress and prospects of hydrogen production: Opportunities and challenges. Journal of Electronic Science and Technology, 19(2), 100080. https://doi.org/10.1016/j.jnlest.2021.100080

[5] Sebbahi, S., Nabil, N., Alaoui-Belghiti, A., Laasri, S., Rachidi, S., & Hajjaji, A. (2022). Assessment of the three most developed water electrolysis technologies: alkaline water electrolysis, proton exchange membrane and solid-oxide electrolysis. Materials Today: Proceedings, 66, 140-145. https://doi.org/10.1016/j.matpr.2022.04.264

[6] Barbir, F. (2005). PEM electrolysis for production of hydrogen from renewable energy sources. Solar Energy, 78(5), 661–669. https://doi.org/10.1016/j.solener.2004.09.003

[7] Kojima, H., Nagasawa, K., Todoroki, N., Ito, Y., Matsui, T., & Nakajima, R. (2023). Influence of renewable energy power fluctuations on water electrolysis for green hydrogen production. International Journal of Hydrogen Energy, 48(12), 4572-4593. https://doi.org/10.1016/j.ijhydene.2022.11.018

[8] Ishaq, H., Dincer, I., & Crawford, C. (2022). A review on hydrogen production and utilization: Challenges and opportunities. International Journal of Hydrogen Energy, 47(62), 26238-26264. https://doi.org/10.1016/j.ijhydene.2021.11.149

[9] Lewinski, K. A., van der Vliet, D., & Luopa, S. M. (2015). NSTF advances for PEM electrolysis: The effect of alloying on activity of NSTF electrolyzer catalysts and performance of NSTF based PEM electrolyzers. ECS Transactions, 69(17), 893–917. https://doi.org/10.1149/06917.0893ecst

[10] Omer, A. M. (2008). Energy, environment and sustainable development. Renewable and Sustainable Energy Reviews, 12(9), 2265-2300. https://doi. org/10.1016/j.rser.2007.05.001

[11] Dai, F., Zhang, S., Luo, Y., Wang, K., Liu, Y., & Ji, X. (2023). Recent progress on hydrogen-rich syngas production from coal gasification. Processes, 11(6), 1765. https://doi.org/10.3390/pr11061765

[12] Barba, D. (2018). Simultaneous production of H2 and sulphur by catalytic oxidative decomposition of H2S. http://dx.doi.org/10.14273/unisa-1321

[13] Kayfeci, M., Keçebaş, A., & Bayat, M. (2019). Hydrogen production. In Solar hydrogen production (pp. 45-83). Academic Press. https://doi.org/10.1016/B978-0-12-814853-2.00003-5

[14] Sayed, E. T., Olabi, A. G., Alami, A. H., Radwan, A., Mdallal, A., Rezk, A., & Abdel kareem, M. A. (2023). Renewable energy and energy storage systems. Energies, 16(3), 141 5. https://doi.org/10.3390/en16031415

[15] Amin, A. M., Croiset, E., & Epling, W. (2011). Review of methane catalytic cracking f or hydrogen production. International Journal of Hydrogen Energy, 36(4), 2904-2935. https:/ /doi.org/10.1016/j.ijhydene.2010.11.035

[16] Guandalini, G., Campanari, S., & Valenti, G. (2016). Comparative assessment and safety issues in state-of-the-art hydrogen production technologies. International Journal of Hydrogen Energy, 41(42), 18901-18920. https://doi.org/10.1016/j.ijhydene. 2016.08.015

[17] Zhao, Z., Situmorang, Y. A., An, P., Chaihad, N., Wang, J., Hao, X., ... & Guan, G. (2020). Hydrogen Production from Catalytic Steam Reforming of Bio-Oils: A Critical Review. Chemical Engineering & Technology, 43(4), 625-640. https://doi.org/10.1002/ceat.201900487

[18] Younas, M., Shafique, S., Hafeez, A., Javed, F., & Rehman, F. (2022). An overview of hydrogen production: current status, potential, and challenges. Fuel, 316, 123317. https://do i.org/10.1016/j.fuel.2022.123317

[19] Nikolaidis, P., & Poullikkas, A. (2017). A comparative overview of hydrogen production processes. Renewable and Sustainable Energy Reviews, 67, 597-611. https://doi.org/10.1016 /j.rser.2016.09.044

[20] Wang, T., Cao, X., & Jiao, L. (2022). PEM water electrolysis for hydrogen production: fundamentals, advances, and prospects. Carbon Neutrality, 1(1), 21. https://doi.org/10.1007/s4 3979-022-00022-8

[21] Muradov, N. Z., & Veziroğlu, T. N. (2005). From hydrocarbon to hydrogen–carbon to hydrogen economy. International Journal of Hydrogen Energy, 30(3), 225–237. https://doi.org/10.1016/j.ijh ydene.2004.03.033

[22] Ikuerowo, T., Bade, S. O., Akinmoladun, A., & Oni, B. A. (2024). The integration of wind and solar power to water electrolyzer for green hydrogen production. International Journal of Hydrogen Energy. https://doi.org/10.1016/j.ijhydene. 2024.02.139

[23] Yang, M., Zhan, Y., Chen, F., Wei, F., Tang, D., Chen, W., ... & Huang, P. (2024). E xisting challenges and development directions of PEM water electrolysis. In Green Hydrog en Production by Water Electrolysis (pp. 108–137). CRC Press. https://doi.org/10.1201/978 1003368939

[24] Zeng, K., & Zhang, D. (2010). Recent progress in alkaline water electrolysis for hydrogen production and applications. Progress in Energy and Combustion Science, 36(3), 307-326. https://doi.org/10.1016/j.pecs.2009.11.002

[25] Rego de Vasconcelos, B., & Lavoie, J. M. (2019). Recent advances in power-to-X techn ology for the production of fuels and chemicals. Frontiers in Chemistry, 7, 454241. https:// doi.org/10.3389/fchem.2019.00392

[26] Athanasaki, G., Jayakumar, A., & Kannan, A. M. (2023). Gas diffusion layers for PEM fuel cells: Materials, properties and manufacturing–A review. International Journal of Hydrogen Energy, 48(6), 2294-2313. https://doi.org/10.1016/j.ijhydene. 2022.10.058

[27] Smolinka, T., Bergmann, H., Garche, J., & Kusnezoff, M. (2022). The history of water electrolysis from its beginnings to the present. In Electrochemical power sources: fundamen tals, systems, and applications (pp. 83-164). Elsevier. https://doi.org/10.1016/B978-0-12-819 424-9.00010-0

[28] Feng, Q., Liu, G., Wei, B., Zhang, Z., Li, H., & Wang, H. (2017). A review of proton exchange membrane water electrolysis on degradation mechanisms and mitigation strategies. Journal of Power Sources, 366, 33-55. https://doi. org/10.1016/j.jpowsour. 2017.09.006

[29] Siahrostami, S., Björketun, M. E., Strasser, P., Greeley, J., & Rossmeisl, J. (2013). Tandem cathode for proton exchange membrane fuel cells. Physical Chemistry Chemical Physics, 15(23), 9326-9334. https://doi.org/10.1039/C3CP51479J

[30] Jahnke, T., Futter, G., Latz, A., Malkow, T., Papakonstantinou, G., Tsotridis, G., ... & K ompis, C. (2016). Performance and degradation of Proton Exchange Membrane Fuel Cells : State of the art in modeling from atomistic to system scale. Journal of Power Sources, 3 04, 207-233. https://doi.org/10.1016/j.jpowsour. 2015.11.041

[31] Lopez, V. M., Ziar, H., Haverkort, J. W., Zeman, M., & Isabella, O. (2023). Dynamic operation of water electrolyzers: A review for applications in photovoltaic systems integration. Renewable and Sustainable Energy Reviews, 182, 113407. https://doi.org/10.1016/j.rser.2023.113407

[32] Chi, J., & Yu, H. (2018). Water electrolysis based on renewable energy for hydrogen pr oduction. Chinese Journal of Catalysis, 39(3), 390-394. https://doi.org/10.1016/S1872-2067(1 7)62949-8

[33] Martinez-Frias, J., Pham, A. Q., & Aceves, S. M. (2001, November). Analysis of a high-efficiency natural gas-assisted steam electrolyzer for hydrogen production. In ASME International Mechanical Engineering Congress and Exposition (Vol. 35524, pp. 565-571). American Society of Mechanical Engineers. https://doi.org/10. 1115/IMECE2001/AES-23667

[34] Chueh, W. C., & Haile, S. M. (2012). Electrochemistry of mixed oxygen ion and electron conducting electrodes in solid electrolyte cells. Annual review of chemical and biomolecular engineering, 3(1), 313-341. https://doi.org/10.1146/annurev-chembioeng- 073009-101000

[35] Hao, S. J., Wang, C., Liu, T. L., Mao, Z. M., Mao, Z. Q., & Wang, J. L. (2017). Fabrication of nanoscale yttria stabilized zirconia for solid oxide fuel cell. International Journal of Hydrogen Energy, 42(50), 29949-29959. https://doi.org/10.1016/j.ijhydene.2017.08.143

[36] Posdziech, O., Schwarze, K., & Brabandt, J. (2019). Efficient hydrogen production for industry and electricity storage via high-temperature electrolysis. International Journal of Hydrogen Energy, 44(35), 19089-19101. https://doi.org/10.1016/j.ijhydene.2018.05.169

[37] Ni, M., Leung, M. K., & Leung, D. Y. (2008). Technological development of hydrogen production by solid oxide electrolyzer cell (SOEC). International Journal of Hydrogen Energy, 33(9), 2337-2354. https://doi.org/10.1016/j.ijhydene.2008.02.048

[38] Zhang, W., Liu, M., Gu, X., Shi, Y., Deng, Z., & Cai, N. (2023). Water electrolysis toward elevated temperature: advances, challenges and frontiers. Chemical Reviews, 123(11), 7119-7192. https://doi.org/10.1021/acs.chemrev.2c00573

[39] Barelli, L., Bidini, G., & Cinti, G. (2018). Steam as sweep gas in SOE oxygen electrode. Journal of Energy Storage, 20, 190-195. https://doi.org/10.1016/j.est. 2018.09.009

[40] Kuterbekov, K. A., Nikonov, A. V., Bekmyrza, K. Z., Pavzderin, N. B., Kabyshev, A. M., Kubenova, M. M., ... & Aidarbekov, N. (2022). Classification of solid oxide fuel cells. Nanomaterials, 12(7), 1059. https://doi.org/10.3390/nano12071059

[41] Kumar, S. S., & Lim, H. (2022). An overview of water electrolysis technologies for green hydrogen production. Energy Reports, 8, 13793-13813. https://doi.org/10.1016/j.egyr.2022.10.127

[42] Sangtam, B. T., & Park, H. (2023). Review on bubble dynamics in proton exchange membrane water electrolysis: Towards optimal green hydrogen yield. Micromachines, 14(12), 2234. https://doi.org/10.3390/mi14122234

[43] Hoerlein, M. P., Riegraf, M., Costa, R., & Schiller, G. (2018). A parameter study of solid oxide electrolysis cell degradation: Microstructural changes of the fuel electrode. Electrochimica Acta, 276, 162-175. https://doi.org/10.1016/j.electacta.2018.04.170

[44] Salehmin, M. N. I., Husaini, T., Goh, J., & Sulong, A. B. (2022). High-pressure PEM water electrolyser: A review on challenges and mitigation strategies towards green and low-cost hydrogen production. Energy Conversion and Management, 268, 115985. https://doi.org/10.1016/j.enconman.2022.115985

[45] Alaswad, A., Omran, A., Sodre, J. R., Wilberforce, T., Pignatelli, G., Dassisti, M., ... & Olabi, A. G. (2020). Technical and commercial challenges of proton-exchange membrane (PEM) fuel cells. Energies, 14(1), 144. https://doi. org/10.3390/en14010144

[46] Apostolou, D., & Xydis, G. (2019). A literature review on hydrogen refuelling stations and infrastructure. Current status and future prospects. Renewable and Sustainable Energy Reviews, 113, 109292. https://doi.org/10.1016/j.rser.2019.109292

[47] Li, H., Guo, J., Li, Z., & Wang, J. (2023). Research progress of hydrogen production technology and related catalysts by electrolysis of water. Molecules, 28(13), 5010. https://doi.org/10.3390/molecules28135010

[48] Terlouw, T., Bauer, C., McKenna, R., & Mazzotti, M. (2022). Large-scale hydrogen production via water electrolysis: a techno-economic and environmental assessment. Energy & Environmental Science, 15(9), 3583-3602. https://doi.org/10. 1039/D2EE01023B

[49] Yu, M., Budiyanto, E., & Tüysüz, H. (2022). Principles of water electrolysis and recent progress in cobalt-, nickel-, and iron-based oxides for the oxygen evolution reaction. Angewandte Chemie International Edition, 61(1), e202103824. https://doi.org/10.1002/anie.202103824

[50] Bajwa, D. S., Pourhashem, G., Ullah, A. H., & Bajwa, S. G. (2019). A concise review of current lignin production, applications, products and their environmental impact. Industrial Crops and Products, 139, 111526. https://doi.org/10.1016/j.indcrop. 2019.111526

[51] Wang, H. Y., Sun, M. L., Ren, J. T., & Yuan, Z. Y. (2023). Circumventing challenges: design of anodic electrocatalysts for hybrid water electrolysis systems. Advanced Energy Materials, 13(4), 2203568. https://doi.org/10.1002/aenm.202203568

[52] Deng, C., Toe, C. Y., Li, X., Tan, J., Yang, H., Hu, Q., & He, C. (2022). Earth-abundant metal-based electrocatalysts promoted anodic reaction in hybrid water electrolysis for efficient hydrogen production: recent progress and perspectives. Advanced Energy Materials, 12(25), 2201047. https://doi.org/10.1002/aenm.202201047

[53] Deng, Y., Chen, N., Feng, C., Wang, H., Zheng, Y., Chen, F., ... & Hu, W. (2019). Degradation of nitrogen-containing refractory organic wastewater using a novel alternating-anode electrochemical system. Science of The Total Environment, 697, 134161. https://doi.org/10.1016/j.scitotenv.2019.134161

[54] Zhang, L., Rao, T. U., Wang, J., Ren, D., Sirisommboonchai, S., Choi, C., ... & Norinaga, K. (2022). A review of thermal catalytic and electrochemical hydrogenation approaches for converting biomass-derived compounds to high-value chemicals and fuels. Fuel Processing Technology, 226, 107097. https://doi.org/10. 1016/j.fuproc.2021.107097

[55] Deng, Y., Zhu, X., Chen, N., Feng, C., Wang, H., Kuang, P., & Hu, W. (2020). Review on electrochemical system for landfill leachate treatment: Performance, mechanism, application, shortcoming, and improvement scheme. Science of the Total Environment, 745, 140768. https://doi.org/10.1016/j.scitotenv.2020.140768

[56] Wang, J. L., & Xu, L. J. (2012). Advanced oxidation processes for wastewater treatment: formation of hydroxyl radical and application. Critical Reviews in Environmental Science and Technology, 42(3), 251-325. https://doi.org/10. 1080/10643389.2010.507698

[57] Zhou, W., Chen, S., Meng, X., Li, J., & Gao, J. (2023). Energy-saving cathodic H2 production enabled by non-oxygen evolution anodic reactions: a critical review on fundament

al principles and applications. International Journal of Hydrogen Energy, 48(42), 15748-157 70. https://doi.org/10.1016/j.ijhydene.2023.01.063

[58] Wang, F., Ouyang, D., Zhou, Z., Page, S. J., Liu, D., & Zhao, X. (2021). Lignocellulosic biomass as sustainable feedstock and materials for power generation and energy storage. Journal of Energy Chemistry, 57, 247-280. https://doi.org/10.1016/j.jechem.2020.08.060

[59] Luo, H., Barrio, J., Sunny, N., Li, A., Steier, L., Shah, N., ... & Titirici, M. M. (2021). Progress and perspectives in photo-and electrochemical-oxidation of biomass for sustainab le chemicals and hydrogen production. Advanced Energy Materials, 11(43), 2101180. https ://doi.org/10.1002/aenm.202101180

[60] Schieppati, D., Patience, N. A., Galli, F., Dal, P., Seck, I., Patience, G. S., ... & Boffito, D. C. (2023). Chemical and biological delignification of biomass: a review. Industrial & Engineering Chemistry Research, 62(33), 12757-12794. https://doi.org/10.1021/acs.iecr.3c01231

[61] You, B., Liu, X., Jiang, N., & Sun, Y. (2016). A general strategy for decoupled hydrogen production from water splitting by integrating oxidative biomass valorization. Journal of the American Chemical Society, 138(41), 13639-13646. https://doi.org/10.1021/jacs.6b07127

[62] Abd El-Sayed, E. S., El-Sakhawy, M., & El-Sakhawy, M. A. M. (2020). Non-wood fibers as raw material for pulp and paper industry. Nordic Pulp & Paper Research Journal, 35(2), 215-230. https://doi.org/10.1515/npprj-2019-0064

[63] Wu, W., Huang, Z. H., & Lim, T. T. (2014). Recent development of mixed metal oxide anodes for electrochemical oxidation of organic pollutants in water. Applied Catalysis A: General, 480, 58-78. https://doi.org/10.1016/j.apcata.2014.04.035

[64] Heinze, T., & Liebert, T. (2001). Unconventional methods in cellulose functionalization. Progress in Polymer Science, 26(9), 1689-1762. https://doi.org/10. 1016/S0079-6700(01)00022-3

[65] Weng, J. K., & Chapple, C. (2010). The origin and evolution of lignin biosynthesis. New Phytologist, 187(2), 273-285. https://doi.org/10.1111/j.1469-8137.2010.03327.x

[66] Yu, X., Yang, B., Zhu, W., Deng, T., Pu, Y., Ragauskas, A., & Wang, H. (2023). Towards functionalized lignin and its derivatives for high-value material applications. Industrial Crops and Products, 200, 116824. https://doi. org/10.1016/j.indcrop. 2023.116824

[67] Eroglu, E., & Melis, A. (2016). Microalgal hydrogen production research. International Journal of Hydrogen Energy, 41(30), 12772-12798. https://doi.org/10. 1016/j.ijhydene.2016.05.115

[68] Yang, Z., Zhou, S., Feng, X., Wang, N., Ola, O., & Zhu, Y. (2023). Recent progress in multifunctional graphene-based nanocomposites for photocatalysis and electrocatalysis application. Nanomaterials, 13(13), 2028. https://doi.org/10. 3390/ nano13132028

[69] Liu, W., Gong, Y., Wu, W., Yang, W., Liu, C., Deng, Y., & Chao, Z. S. (2018). Efficient Biomass Fuel Cell Powered by Sugar with Photo-and Thermal-Catalysis by Solar Irradiation. ChemSusChem, 11(13), 2229-2238. https://doi.org/10.1002/cssc. 201800719

[70] Holade, Y., Tuleushova, N., Tingry, S., Servat, K., Napporn, T. W., Guesmi, H., ... & Kokoh, K. B. (2020). Recent advances in the electrooxidation of biomass-based organic molecules for energy, chemicals and hydrogen production. Catalysis Science & Technology, 10(10), 3071-3112. https://doi.org/10.1039/C9CY02446H

[71] Tong, Y., Xu, B., & Ye, F. (2024). Recent Advance in Solution-Processed Hole Transporting Materials for Organic Solar Cells. Advanced Functional Materials, 34(10), 2310865. https://doi.org/10.1002/adfm.202310865

[72] Horn, M. R., Singh, A., Alomari, S., Goberna-Ferrón, S., Benages-Vilau, R., Chodankar, N., ... & Dubal, D. (2021). Polyoxometalates (POMs): from electroactive clusters to energy materials. Energy & Environmental Science, 14(4), 1652-1700. https://doi.org/10.1039/D0EE03407J

[73] Yang, L., Liu, W., Zhang, Z., Du, X., Gong, J., Dong, L., & Deng, Y. (2017). Hydrogen evolution from native biomass with Fe3+/Fe2+ redox couple catalyzed electrolysis. Electrochimica Acta, 246, 1163-1173. https://doi.org/10.1016/j.electacta. 2017.06.124

[74] Chen, C., Fu, Z., Qi, F., Chen, Y., Meng, G., Chang, Z., ... & Shi, J. (2022). Fe2+/Fe3+ Cycling for Coupling Self-Powered Hydrogen Evolution and Preparation of Electrode Catalysts. Angewandte Chemie International Edition, 61(32), e202207226. https://doi.org/10.1002/anie.202207226

[75] Christopher, L. P., Yao, B., & Ji, Y. (2014). Lignin biodegradation with laccase-mediator systems. Frontiers in Energy Research, 2, 12. https://doi.org/10.3389/fenrg. 2014.00012

[76] Zhang, C., Shen, X., Jin, Y., Cheng, J., Cai, C., & Wang, F. (2023). Catalytic strategies and mechanism analysis orbiting the center of critical intermediates in lignin depolymerization. Chemical Reviews, 123(8), 4510-4601. https://doi.org/10.1021/acs.chemrev.2c00664

[77] Sánchez, M., Amores, E., Abad, D., Rodríguez, L., & Clemente-Jul, C. (2020). Aspen Plus model of an alkaline electrolysis system for hydrogen production. International Journal of Hydrogen Energy, 45(7), 3916-3929. https://doi.org/10.1016/j.ijhydene.2019.12.027

[78] Sánchez, M., Amores, E., Rodríguez, L., & Clemente-Jul, C. (2018). Semi-empirical model and experimental validation for the performance evaluation of a 15 kW alkaline water electrolyzer. International Journal of Hydrogen Energy, 43(45), 20332-20345. https://doi.org/10.1016/j.ijhydene.2018.09.029

[79] Abdin, Z., Webb, C. J., & Gray, E. M. (2017). Modelling and simulation of an alkaline electrolyser cell. Energy, 138, 316-331. https://doi.org/10.1016/j.energy.2017.09.053

[80] U.S. Energy Information Administration. (2026). Electric Power Monthly: Table 5.3. Average price of electricity to ultimate customers: Total by end-use sector. U.S. Energy Information Administration. https://www.eia.gov/electricity/monthly/epm_table_grapher.php?t=table_5_03

[81] International Energy Agency. (2026). Electricity 2026: Prices. International Energy Agency. https://www.iea.org/reports/electricity-2026/prices

[82] Umer, M., Brandoni, C., Tretsiakova, S., Hewitt, N., Dunlop, P., Mokim, M. D., Zhang, K., & Huang, Y. (2024). Hydrogen production through polyoxometalate catalysed electrol ysis from biomass components and food waste. Results in Engineering, 23, 102803. https:/ /doi.org/10.1016/j.rineng.2024.102803